Array Element Localisation

Locating array elements in underwater environment using the sound from a powerboat

Olle Bristedt
Axel Sundberg

A master's thesis presented for the degree of
M Sc. Industrial Engineering and Management

Mathematical Statistics
Lund University
Sweden
June 2017

Abstract

This thesis have been written in cooperation with the Swedish Defense Research Agency (FOI). The thesis is concerned with calibration of hydrophone positions, or Array Element Localisation (AEL). Data from two experiments have been provided by FOI, one where the hydrophones have been pinged with a narrowband signal and one where the array have been circled by a powerboat. The model currently used by FOI applies the pinged data and this model have been evaluated and compared to two extended models. However, the primary purpose have been to develop a novel algorithm for AEL using sound generated from a powerboat. In order to accomplish this, several different algorithms have been developed and evaluated in both a simulated environment and on real data. The essence of the developed models for AEL with powerboat data, is optimisation over the output of a delay-and-sum beamformer. Comparison to the result of AEL using pings show that the developed model performs well for one out of two arrays.

Acknowledgement

The authors of this Master's Thesis would like to thank Erik Gudmundson at the Swedish Defence Research Agency for the opportunity to participate in this project. Erik has provided essential in-depth knowledge in the subject and guided us through the process of building the mathematical models. Furthermore, Andreas Jakobsson, Head of division, Centre for Mathematical Sciences Mathematical Statistics, Lund Institue of Technology, is thanked for splendid mentoring throughout the creation of this thesis.

Contents

General notation

The notation that is consistently used throughout the thesis is introduced in table 1.1. The notation is consistent in the sense that it always refers to the same concept, although the dimension may change in different sections. For example, $\boldsymbol{p}$ always refers to coordinates of a hydrophone, but if $\boldsymbol{p}$ is in two or three dimension depends on the context.

Notation	**Explanation**
N	Number of hydrophones
M	Number of send locations
$\boldsymbol{p}_n$	Coordinates of hydrophone n
c	Medium propagation speed (constant)
$\boldsymbol{a}$	Array transfer vector
$x(t)$	Input signal, time domain
$X(\omega)$	Input signal, frequency domain
$\boldsymbol{y}(t)$	Output signal, time domain
$\boldsymbol{Y}(\omega)$	Output signal, frequency domain
θ	Direction of arrival
τ_n	Difference in arrival time between sensor 1 and sensor n

Table 1.1: *General notation*

Abbreviation	**Explanation**
AEL	Array Element Localisation
$AELUP$	Array Element Localisation using Pings
$AELUP-MM$	Array Element Localisation using Pings - Moving Model
$AELUP-CM$	Array Element Localisation using Pings - Constrained Model
DOA	Direction Of Arrival
FFT	Fast Fourier Transform
ROV	Remotely Operated underwater Vehicle
GPS	Global Positioning System
FOI	Swedish Defence Research Agency

Table 1.2: *Abbreviations*

Introduction

Ever since World War I, the submarine have been an essential piece of naval warfare. With the introduction of underwater vessels, the need for underwater surveillance increased dramatically and still occupy the minds of intelligence agencies around the world. The developed surveillance techniques can also be used in non-military applications such as deep-sea pollution monitoring, assessing impacts of offshore infrastructure on local ecosystems and oil leakage control.

One primary tool for underwater surveillance is the study of sound propagation under water. The acoustic signals are measured by microphones underwater, so-called hydrophones, and the received signal is then treated mathematically to, for example, detect passing submarines. In order to accomplish this, several hydrophones are usually placed together and synchronised into what is called arrays. This thesis, written in cooperation with the Swedish Defense Research Agency (FOI), aims to calibrate the hydrophone positions of two such arrays in order to improve performance. Calibration of hydrophone positions is in the literature, and throughout this thesis, referred to as Array Element Localisation (AEL).

The focus of this thesis is on the exact positions of the hydrophones in an array. To have the exact positions is highly important since even small errors in the hydrophone positions can introduce biases when using the array in practice. The arrays of interest are passive arrays on the sea floor, which, for estimation purposes, are about a hundred meters long and consist of more than fifty hydrophones. When placing the array on the sea floor, it needs to be sunk. Due to the arrays size, waves and currents, this may cause the geometry of the array to shift. Therefore, there is a need to calibrate the array by estimating the exact hydrophone positions within the array.

The current calibration method used by FOI is to, from the surface, transmit a ping (a loud and short signal) toward the array. Each hydrophone will then record the transmitted signal as a spike in the data. From the difference in arrival times of the spike, it is possible to determine the relative positions. However, there are two reasons why this method is undesirable. Firstly, since there are many arrays to be calibrated, it is expensive due to requirement of expensive equipment and staff to conduct experiments at each array. Secondly, military intelligence often prefer clandestine operations, and the loudness of the signal impairs the ability to, for example, keep the array position secret.

The aim of this thesis is to develop a method to calibrate the hydrophone positions

without the use of pings. Instead, data have been collected from an experiment where a powerboat drove around the two arrays. The developed method primarily builds upon a mathematical technique called beamforming.

2.1 Problem Formulation

This thesis focuses exclusively on positioning hydrophone elements within the two arrays. In doing so there are two problems that have been considered, these are:

1. Is it possible to improve upon the existing Array Element Localusation using pings algorithm (AELUP)?
2. Can the positioning of hydrophones be accomplished using the sound from a powerboat?

2.2 Structure of the thesis

The thesis can be considered to have two main parts divided as the problem formulation would suggest. The first part considers models based on ping data. It starts with a description of the arrays that have been used in the experiment and then describes the model currently used by FOI, AELUP. Furthermore, two extensions of the AELUP algorithm are considered.

The main focus of the report is on the second part which considers the powerboat data. This section starts by describing the theory behind the developed model, in particular beamforming. Thereafter, it describes the data that has been provided by FOI. Afterwards comes a section describing the results from the developed model in a simulated environment. Finally, the results are presented, followed by a discussion.

Array description

The two arrays that are to be positioned consists of 56 hydrophones each and are referred to as *Pass1* and *Pass2*. The hydrophones, also referred to as *elements*, *channels* and *sensors*, are all attached to a flexible cord which is connected to a computer, that processes the signal received. In figure 3.1, a linear hydrophone array is depicted. The depicted array is not the same as the one used in practice but gives the reader a sense of what a hydrophone array looks like and how flexible it is.

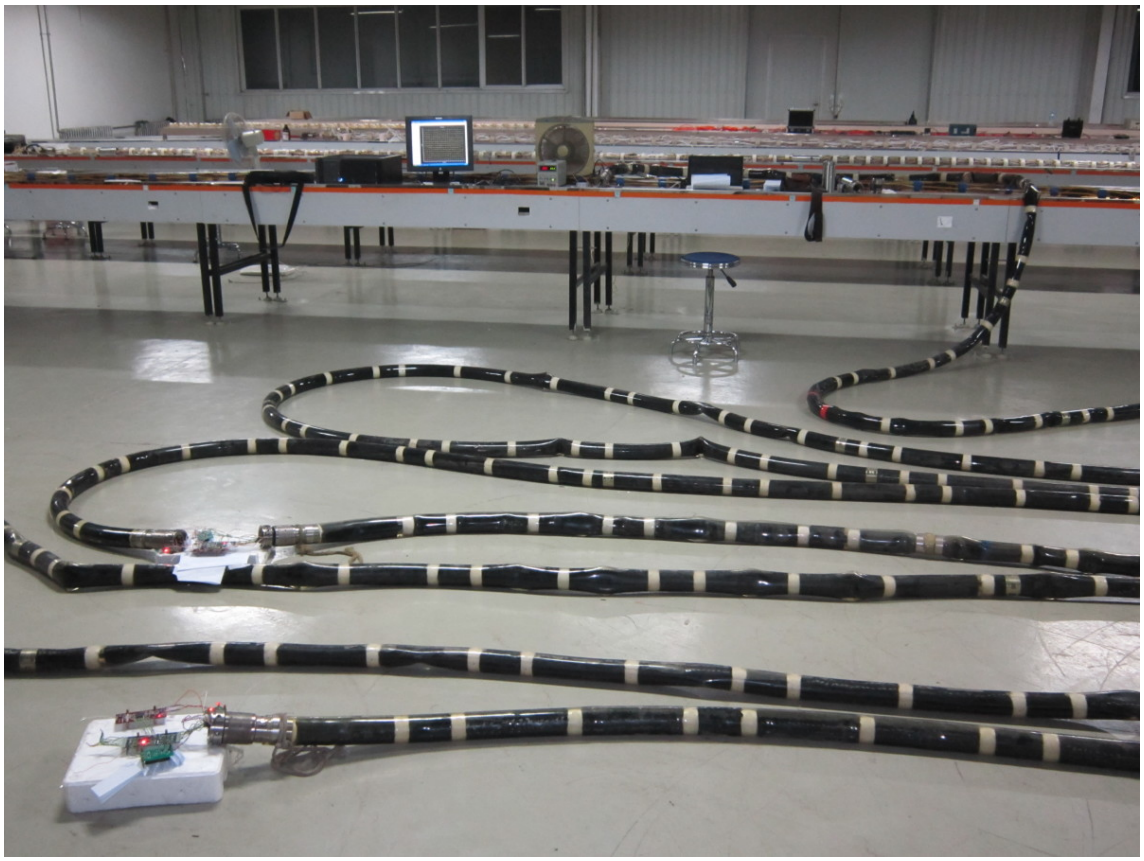

Figure 3.1: *Picture of linear array in laboratory. Source: Chen et al. 2013*

The arrays have both been anchored to the sea floor on one end and the first hydrophone is located in the proximity of the anchor. There is much greater certainty in the position of the anchor, and therefore the position of the first hydrophone is compared relative to the other positions. Because of this relation, the position of the first hydrophone in each of the two arrays is fixated. The fixation simplifies the

problem since it is now sufficient to get the remaining hydrophone positions relative to the first.

3.1 Design frequency

The linear array used in the experiment can also be seen as six nested uniform linear arrays. Each of the arrays follow equation (3.1)-(3.3), where λ is the signal wave-length, c is the medium propagation speed, ω is the signal frequency and d is a distance. The reason why the nested representation would be more preferable is explained by equation (3.3), which is obtained by combining (3.1) and (3.2). The equation relates the distance, d, between the hydrophones in the linear array to frequencies where the optimal resolution, so-called *design frequencies*, for detection lobes is obtained (Rabinovich and Alexandrov 2012). In table 3.1, the hydrophone nests and their corresponding design frequency are displayed. The hydrophones are numbered such that hydrophone 1 is the hydrophone located closest to the anchor and hydrophone 56 furthest away. The reason for arranging the array in nests is to have high resolution for more than one frequency and detect various vessels.

$$\lambda = \frac{c}{\omega} \tag{3.1}$$

$$d = \frac{\lambda}{2} \tag{3.2}$$

$$d \leqslant \frac{c}{2 \cdot \omega} \tag{3.3}$$

	Distance (m)	Design Frequency (Hz)
Hyd: 1-17	0.234	3200
Hyd: 1,3,5,7,9,11,13,15,17-24	0.469	1600
Hyd: 1,5,9,13,17,19,21,23,25-33	0.938	800
Hyd: 1,9,17,21,25,27,29,31,33-40	1.875	400
Hyd: 1,17,25,29,33,35,37,39,41-49	3.750	200
Hyd: 1,25,33,37,41,43,45,47,49-56	7.500	100

Table 3.1: *Hyd 1 is the hydrophone closest to the anchor and hyd 56 is the hydrophone furthest away from the anchor. The table presents the six different nests formed by hydrophones in the array. The itended distance between hydrophones and corresponding design frequency for optimal detection lobes under the assumption of constant sound speed, $c = 1500\ m/s$.*

.

3.2 Medium propagation speed

A crucial assumption of this report is that the speed of sound under water, referred to as the medium propagation speed, is constant. In general, this cannot be claimed to be true as there are many factors that affect the speed of sound, such as: depth, temperature, wind, and salinity. The rule of thumb for the speed of sound underwater is that it is around 1500 m/s, but thanks to an experiment conducted by FOI around the time of the experiment the value is more accurately known. From

figure 3.2 it is concluded that the speed of sound is constant around 1435 m/s, the experiment also showed that the propagation speed is fairly constant from the sea floor to the surface. Hence, from this point forward, the speed of sound, denoted c, is assumed constant and equal to 1435 m/s. The updated estimate for the speed of sound also decreases the design frequencies in table 3.1 according to equation (3.3).

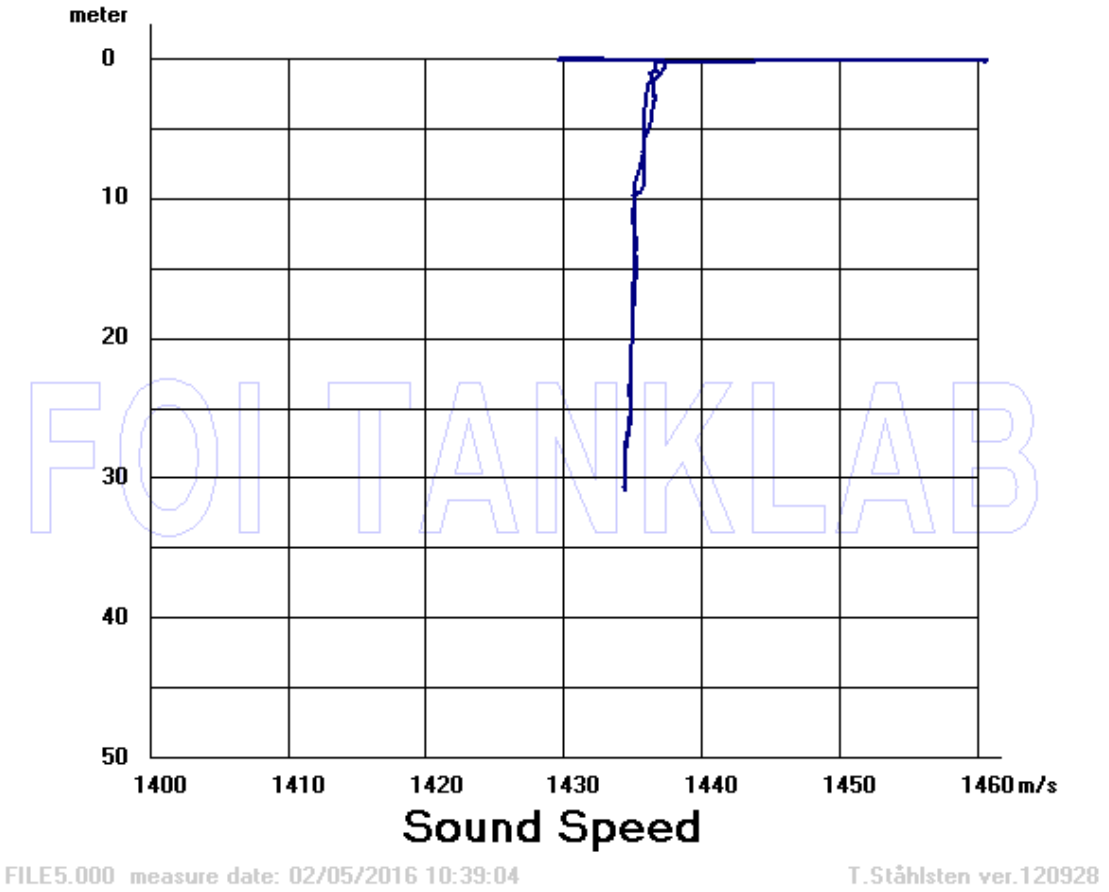

Figure 3.2: *Speed of sound profile at array location, experiment conducting by FOI 2016-05-02. Source: FOI*

Array Element Localisation using Pings

The model described in this chapter builds upon measurements where the hydrophones have been pinged with a narrowband signal. The model is referred to as the AELUP algorithm and is the model currently used by FOI. Despite being previously developed it is of interest for the reader since it is the reference point to which other models have been evaluated. The great advantage of having data where the hydrophone have been pinged is that it is possible to measure a distinct arrival time of each pulse (or ping).

4.1 Model description

In figure 4.1 the notation is introduced and the setting laid out. To ease notation, the theory of the AELUP algorithm is explained in a two dimensional setting. When implemented in practice the sea floor was assumed to be flat, implying that this representation is not restrictive. Using the notation in figure 4.1, it is easily realised

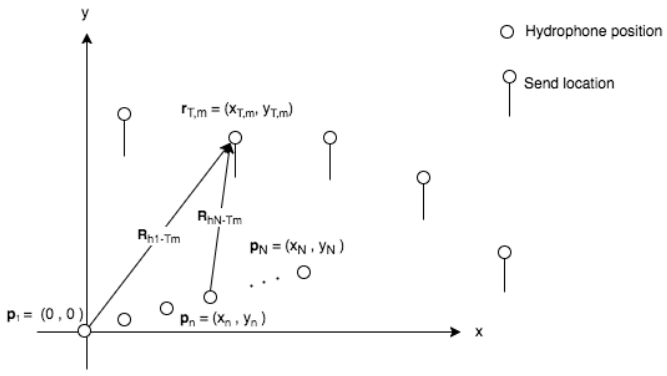

Figure 4.1: *AELUP model setting.*

that the length of the vectors can be calculated according to equations (4.1) and (4.2).

$$r_{h1-Tm} = \frac{1}{c} \cdot \sqrt{(x_1 - x_{Tm})^2 + (y_1 - y_{Tm})^2} \tag{4.1}$$

$$r_{hn-Tm} = \frac{1}{c} \cdot \sqrt{(x_n - x_{Tm})^2 + (y_n - y_{Tm})^2} \tag{4.2}$$

where c is the medium propagation speed, and r_{hn-Tm} is the distance from the hydrophones to the send locations of the sound. Now, denoting the measured arrival

times as (4.3) we can calculate the difference in arrival times between hydrophone 1 and hydrophone n, i.e., τ_{nm} as in (4.4).

$$t_{nm} = \text{Time for pulse } m \text{ to reach hydrophone } n \tag{4.3}$$

$$\tau_{nm} = t_{1m} - t_{nm} \tag{4.4}$$

For an assumed position of a sensor n, $n = [2, 3, ..., N]$, we can also calculate τ_{nm} as:

$$\begin{aligned} \tau_{nm} &= \frac{1}{c} \cdot (r_{h1-Tm} - r_{hn-Tm}) \Leftrightarrow \\ \tau_{nm} \cdot c - r_{h1-Tm} + r_{hn-Tm} &= 0 \end{aligned} \tag{4.5}$$

Using equation (4.5), we are now able to construct an objective function to find the hydrophone positions, $\mathbf{P}$, where $\boldsymbol{P} = [\boldsymbol{p}_2 \quad \boldsymbol{p}_3 \dots \boldsymbol{p}_N]$ and $\boldsymbol{p}_n = (x_n, y_n)$ denotes the position of hydrophone n. The objective function is defined in equation (4.6), where clearly $\boldsymbol{p}_n$ enters through the calculation of r_{hn-Tm}.

$$\underset{\boldsymbol{p}_2, \boldsymbol{p}_3, \dots, \boldsymbol{p}_N}{\text{minimise}} \quad \sum_{m=1}^{M} \sum_{n=2}^{N} \left\| \tau_{nm} \cdot c - r_{h1-Tm} + r_{hn-Tm}(\boldsymbol{p}_n) \right\|^2 \tag{4.6}$$

4.2 Method

The methodology for Array Element Localisation using Pings, (AELUP) algorithm was entirely developed by FOI and is not the main focus of this thesis. However, since the results are used for comparison to all other estimations there are some aspects of how the experiment was conducted that make trade-offs, made later in the thesis, more logical. Therefore, in this section the aim is to briefly describe, to the best of our understanding, how the experiment was conducted.

4.2.1 Description of experiment

The method to estimate AEL with pinged data, builds upon sending a pulse from a known location toward the array and when the pulse reaches the hydrophones an easily identifiable spike will be present in the data. As described in section 4.1, if the send time and arrival time of the pulse is known, an algorithm can be designed to position each array element.

To increase the accuracy of the algorithm, a total of 16 send locations, or clusters, were used and from each cluster about 150 pulses were sent. The position of the boat at each location was recorded by two different GPS, one hand-held and one boat-mounted. At each cluster the aim of the crew conducting the experiment was to be as still as possible, but considering currents and wind this is difficult to achieve. Therefore, some drift inside the cluster can be expected, this drift can be expected to be constant since currents and waves generally do not change within short time periods.

To generate the pulse a sound generating device, lowered into the water. The current model assumed that the position of this transmitter is the same as the GPS

coordinate generated on board. Each pulse generated is of the shape in figure 4.2 a) having a spectrum as shown in figure 4.2 b).

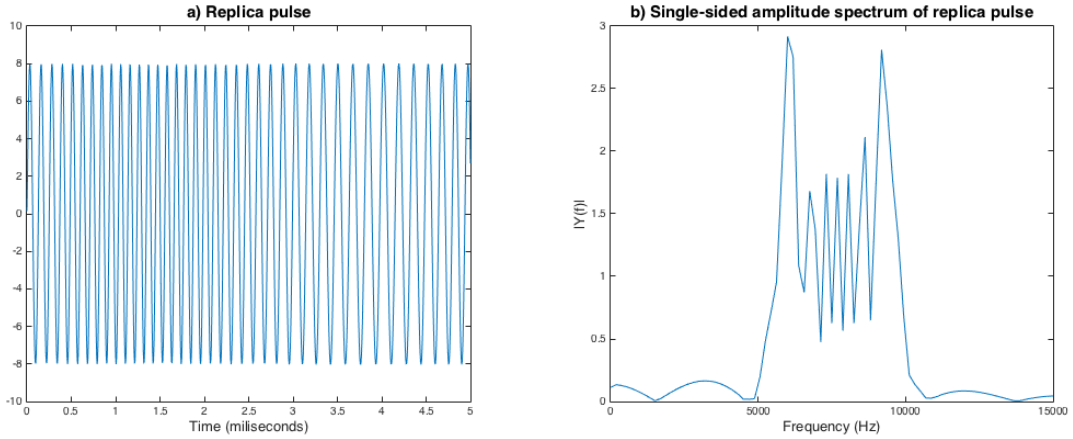

Figure 4.2: *a) The pulse sent from each send location in time domain b) The same pulse but in the frequency domain.*

4.2.2 Estimation of Arrival Times

To estimate the exact arrival time based on pings is not as obvious as it may seem at first glance. One reason is that the pulse recorded by the hydrophones will be corrupted by background noise. The method applied by FOI is to apply the Hilbert transform combined with a matched filter of the replica pulse. In theory this would generate a precise spike in the output at the time the pulse was registered. The actual results turned out as several high peaks, grouped together. The selection of which peak to deem as the true arrival time of the signal is problematic and creates ambiguity.

Practical experience at FOI has shown that the first flank of the peak generally works well. To find this flank, a threshold value was manually decided upon and thereafter the corresponding time index was extracted from the data. In this project, the arrival times FOI found by this method have been applied. It has also been shown that the impact of changing from the flank value to, for example the highest peak value, have limited impact on the results.

4.3 Result

To solve the optimisation problem in (4.6), the built-in MatLab routine *fsolve* was used. The algorithm did not converge but stopped prematurely since the last step taken by the algorithm was ineffective as defined by the function tolerance. The results, provided by FOI, are displayed in figure 4.3.

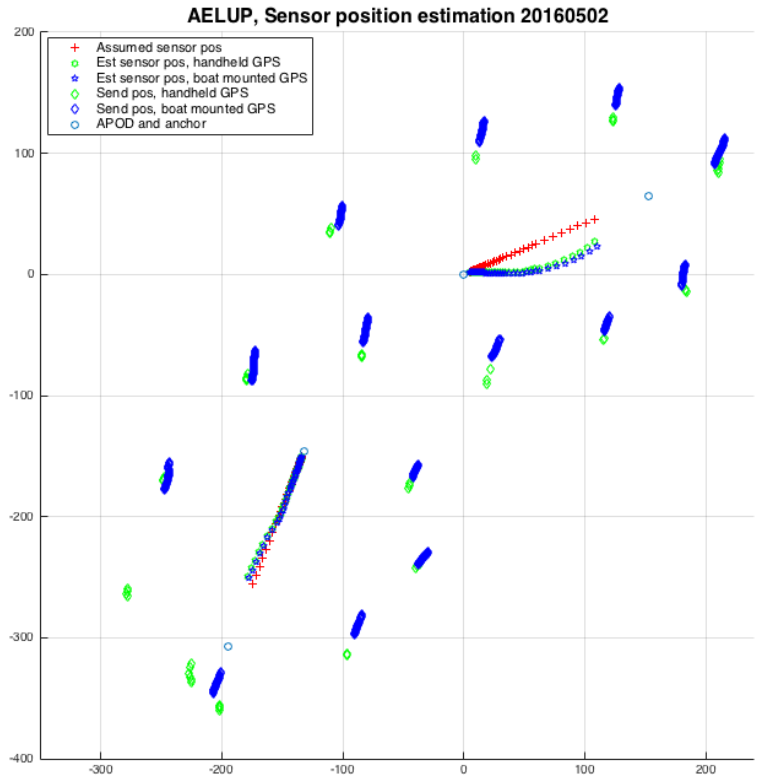

Figure 4.3: *Result of the AELUP algorithm. The 16 clusters are shown around the two arrays estimated by pings sent from the clusters.*

In table 4.1, the distances between estimated hydrophone positions are shown for positions were the distance have been estimated as greater than the maximum distance possible. The maximum distance restriction comes from the attachment of the hydrophones to the cord, see section 3. Hence, table 4.1 can be considered proof that the AELUP algorithm estimates are not 100 % accurate.

4.4 Discussion

The results show that there is quite some difference between the assumed and the estimated positions, especially in the top-corner array (Pass1). This will later turn out to be problematic for the beamform calibration method.

Furthermore, regardless if the hand-held or boat-mounted GPS trace is used the estimated hydrophone positions converges to almost the same locations. This clearly strengthens the credibility of the results since thus appear to be robust. Considering both GPS traces, it appears as if the boat-mounted moves more as expected, see section 4.2.1. This observation have been confirmed by FOI; the boat mounted GPS is known by them to be more accurate since it uses a Differential Global Positioning System (DGPS). The difference to ordinary GPS is that in addition to satellite triangulation it uses ground based stations on fixed locations. Therefore, from this point forward the boat mounted GPS trace will be preferred.

Pass1			Pass2		
Hyd	d	Max d	Hyd	d	Max d
2	0.290	0.234	4	0.256	0.234
3	0.235	0.234	7	0.235	0.234
8	0.248	0.234	9	0.269	0.234
16	0.489	0.469	11	0.275	0.234
24	0.948	0.938	13	0.243	0.234
36	1.891	1.875	14	0.239	0.234
51	7.745	7.500	15	0.255	0.234
			16	0.606	0.469
			22	0.513	0.469
			25	0.945	0.937
			30	0.941	0.938
			36	1.889	1.875
			38	1.904	1.875
			45	3.754	3.750
			47	3.857	3.750
			49	7.529	7.500

Table 4.1: *Distance between estimated hydrophone positions were the distance is greater than the maximum distance. Column with label d marks the estimated distance and max d the maximum distance between the hydrophones. The column Hyd refers to the distance between hydrophone n+1 and n.*

The result have also been confirmed with a ROV (Remotely Operated Underwater Vehicle) by FOI. From that investigation, it was concluded that the estimated positions are "good enough". Despite the investigation it is not possible to claim that the positions are completely accurate, this is due to that some distances between the hydrophones are small (less than half a meter) and therefore the GPS-trace that the ROV generates is not accurate enough to give precise positions, which is evident from table 4.1. However, from the ROV, the shape of the estimated positions is confirmed to be correct. Since the results from the model is not 100% reliable the results of this sections will be referred to as 'Estimated positions, AELUP' rather than 'True positions'.

Array Element Localisation using Pings - Moving Model

One suggestion for improvement of the pinged data estimation algorithm was to build a model for the movement of the transmitter. This is due to that the transmitter, which generates the pulse, is located some distance into the water from the position of the boat were the GPS is mounted. Hence, it is a rather strong assumption to claim that the transmitter has the same GPS coordinates as the boat. With some minor model adaptation this assumption can be relaxed to that the sender *moves* in the same direction as the boat within a given cluster. The assumption is likely to hold well if the boat drifts at constant speed, but if it were to change direction it would immediately be violated. There is some intuition for why the boat would be drifting at constant speed, see section 4.2.1. The Array Element Localisation using Pings - Moving Model is referred to as *AELUP-MM*.

5.1 Model Description

The model set up is explained in figure 5.1. By assuming that the transmitter moves in the same direction as the boat the problem of ambiguity in the send location is reduced to only one position per cluster (x_{op}, y_{op}) in the figure. The speeds, v_x and v_y, are easily estimated from the GPS coordinates, as in equations (5.1) and (5.2).

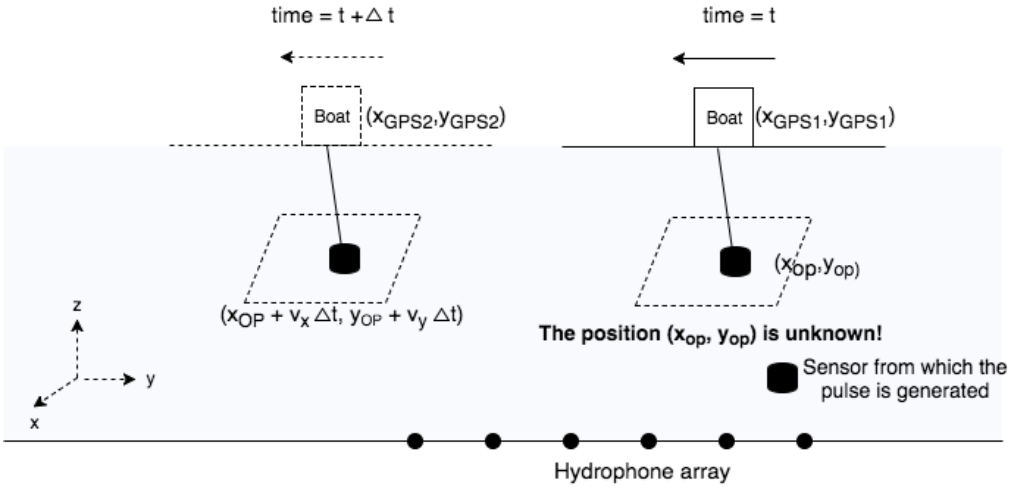

Figure 5.1: *Array Element Localisation using Pings - Moving Model set up.*

$$v_{x_m} = \frac{1}{\Delta t} \cdot (x_{GPS_{t_m}} - x_{GPS_{t_{m-1}}}) \tag{5.1}$$

$$v_{y_m} = \frac{1}{\Delta t} \cdot (y_{GPS_{t_m}} - y_{GPS_{t_{m-1}}}) \tag{5.2}$$

Above, the Δt refers to the time between two consecutive pulses of the transmitter. What remains before the AELUP-MM can be applied is a slight change of the calculations for the distances r_{h1-tm} and r_{hn-Tm}, see equations (4.1) and (4.2). The new equations become as in (5.3) and (5.4). The index q, $q = [1 \quad 2 \ldots 16]$ denotes the cluster pulse m belongs to.

$$r_{h1-Tm} = \frac{1}{c} \cdot \sqrt{(x_{h1} - (x_{op_q} + v_x \cdot \Delta t))^2 + (y_{h1} - (y_{op_q} + v_{y_m} \cdot \Delta t_m))^2} \tag{5.3}$$

$$r_{hn-Tm} = \frac{1}{c} \cdot \sqrt{(x_{hn} - (x_{op_q} + v_x \cdot \Delta t))^2 + (y_{hn} - (y_{op_q} + v_{y_m} \cdot \Delta t_m))^2} \tag{5.4}$$

If we define r_{op} as in equation (5.5) the objective function becomes as in equation (5.6).

$$\boldsymbol{r}_{op_q} = (x_{op_q}, y_{op_q}) \tag{5.5}$$

$$\underset{\boldsymbol{p}_2, \boldsymbol{p}_3 \ldots, \boldsymbol{p}_N, \boldsymbol{r}_{op_1}, \ldots \boldsymbol{r}_{op_{16}}}{\text{minimise}} \quad \sum_{m=1}^{M} \sum_{n=2}^{N} \left\| \tau_{nm} \cdot c - r_{h1-Tm}(\boldsymbol{r}_{op_q}) + r_{hn-Tm}(\boldsymbol{p}_n, \boldsymbol{r}_{op_q}) \right\|^2 \tag{5.6}$$

5.2 Result

To solve the problem in (5.6), the MatLab built-in routine fsolve was used. Again, the optimisation did not converge but stopped prematurely at the function evaluation limit. In figure 5.2, the results from the AELUP-MM are compared to the ones from AELUP.

5.3 Discussion

The results shown in figure 5.2 show that the AELUP-MM yields similar estimates as the AELUP algorithm. Clearly, this is satisfying as the ROV has proven that those results are at least close to the actual hydrophone positions. Furthermore, the estimation of r_{op} are in line with the boat GPS positions for that cluster.

Eventually it was decided, by FOI, to stick with the AELUP estimates as the key when later implementing the proposed beamforming algorithm. The reason for this is that the trade-off between complexity and accuracy in positioning is not clear due to an unknown error in the AELUP-MM algorithm.

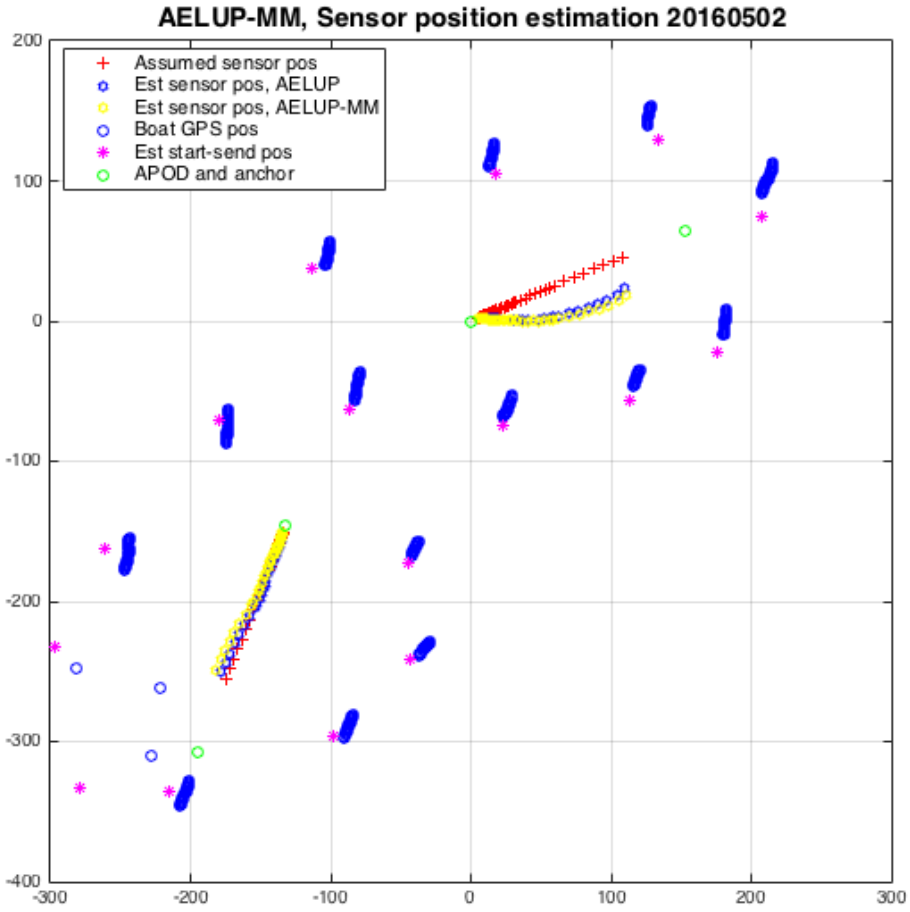

Figure 5.2: *Result of the AELUP-MM algorithm. The optimisation stopped prematurely for the AELUP-MM algorithm in positions close to the estimates from the AELUP algorithm.*

Array Element Localisation using Pings - Constrained Model

If one studies table 4.1, it is clear that there are some violations of the maximum distance which can occur between two hydrophones. Since this is a physical constraint, it makes sense to build a model which prohibits the algorithm to choose such positions. The Array Element Localisation using Pings - Constrained Model, abbreviated *AELUP-CM*, is such a model.

6.1 Model Description

The AELUP-CM algorithm is similar to the AELUP algorithm except for that boundary conditions are included. The boundary conditions can be seen as that hydrophone $n+1$ cannot be further away from hydrophone n than the actual distance between those two hydrophones on the array line to which they are attached. However, since the array is flexible and can bend it, is possible for hydrophones to be closer to each other than the intended distance.

The boundary conditions described above are illustrated in figure 6.1 below, where a snapshot of what it theoretically could look like in one iteration step of the algorithm. The picture is not intended to show the actual inner workings of the algorithm, which may break the boundary conditions at times to speed up convergence, but rather illustrate the idea behind the conditions. A mathematical formulation of

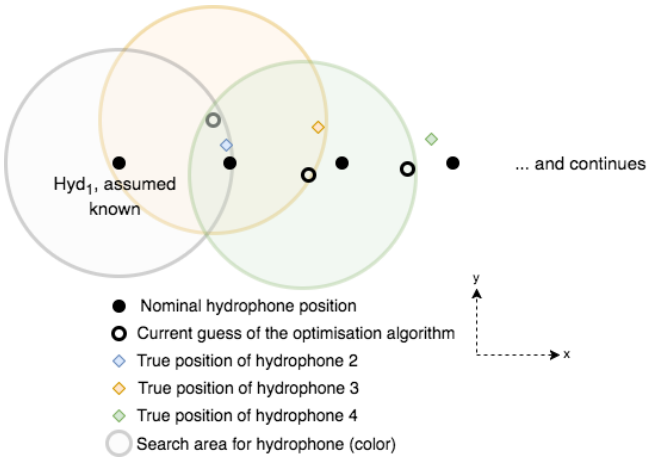

Figure 6.1: *Snapshot of one iteration and allowed search areas for the iteration step in the constrained model.*

the objective function with boundary conditions is displayed in equation (6.1). The objective function is now a high dimensional non-linear constrained optimisation problem with multiple non-linear boundary conditions. As in the current model r_{h1-Tm} and r_{hn-Tm} are defined as in equations (4.1) and (4.2) and $p_n = (x_n, y_n)$. d_n denotes the design distance between hydrophone $n+1$ and n. The design distances are displayed in table 3.1.

$$\begin{aligned} &\underset{\boldsymbol{p}_2,\boldsymbol{p}_3\cdots,\boldsymbol{p}_N}{\text{minimise}} \quad -\sum_{m=1}^{M}\sum_{n=2}^{N} \|\tau_{nm}\cdot c - r_{h1-Tm} + r_{hn-Tm}(\boldsymbol{p}_n)\|^2 \\ &\text{subject to} \quad \sqrt{(x_{n+1}-x_n)^2+(y_{n+1}-y_n)^2} \leqslant d_n,\ n = 2,\ldots,N-1. \end{aligned} \tag{6.1}$$

6.2 Result

Again the built in routine in the MatLab optimisation toolbox *fsolve* was used to solve the optimisation problem (6.1). Neither this time did the optimisation converge before the function evaluation limit was reached. The results obtained for the AELUP-CM compared to the results of the AELUP algorithm is displayed in figure 6.2.

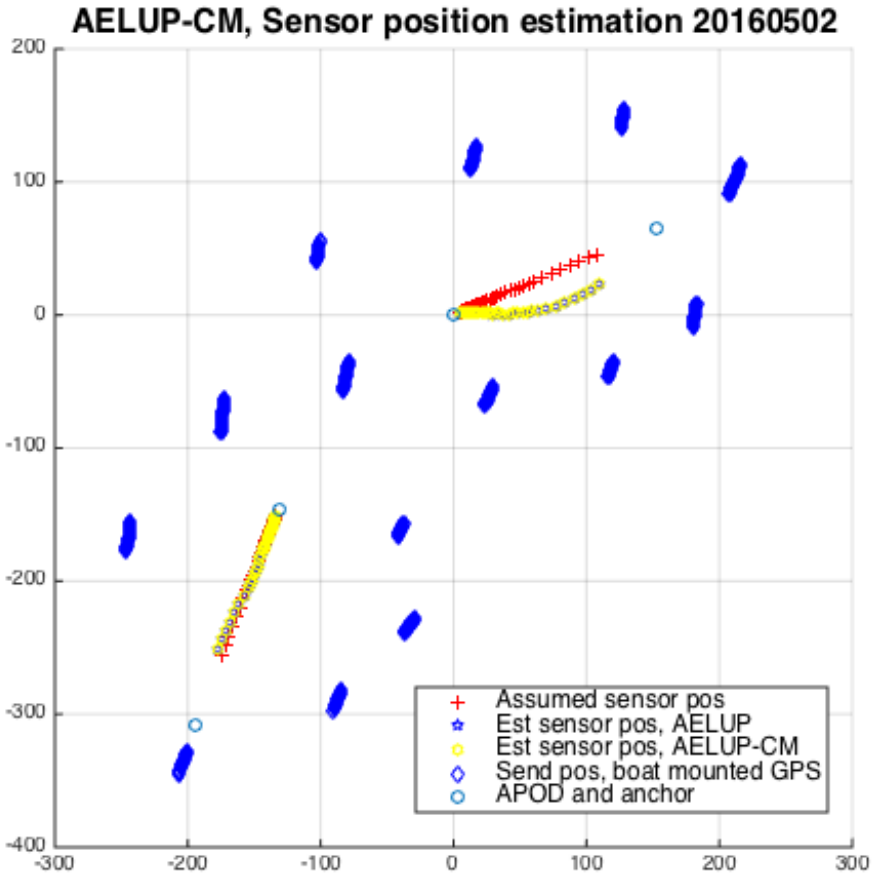

Figure 6.2: *Results of the AELUP-CM.*

6.3 Discussion

The credibility of the AELUP algorithm is again confirmed by the constrained model, which converges to positions close to the estimates of the AELUP algorithm. In theory, the constrained model should be preferred since it is a better abstraction of the real world problem. The results are also satisfying in the sense that the boundary conditions are not violated. However, in discussion with FOI it was decided to keep the AELUP algorithm for comparative purposes. The reason is that their practical experience from working with nonlinear constrained optimisations algorithms is that they tend to converge to estimates on, or very close to, the boundary.

Theory

In this chapter the, for this thesis essential theory behind beamforming is explained. Most of the theory is based upon (Stoica and Moses 2005, chapter 5) and (Van Trees 2004, chapter 2). The aim is to provide the necessary theory to formulate an objective function for AEL based on continuous signals from a powerboat.

7.1 Uniform Linear Array Model

Estimating direction of arrivals, DOA, of signals is a large field of research and have many applications in for example radar systems. In a DOA problem, the locations of the sensor elements are assumed to be known as well as the measured output of each sensor. In many situations, it is adequate to use a uniform linear array, ULA, see figure 7.1. In the ULA, it is assumed that each sensor is placed on equidistant nodes with spacing d. For simplicity, we initially consider the case when only one source is present.

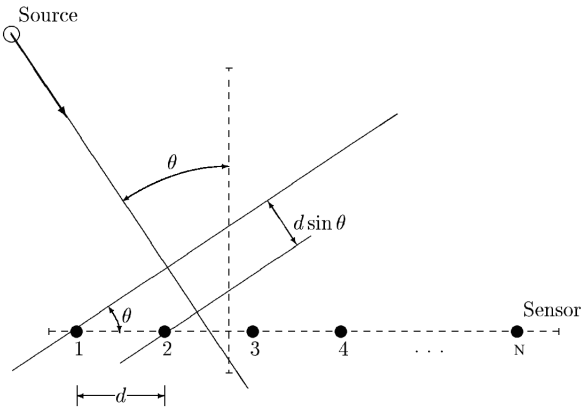

Figure 7.1: *The uniform linear array setup where the direction of arrival is defined as the angle between the normal to the array and the source location. Source Stoica and Moses 2005 p.284*

.

In this model, the signal source is assumed to be in the far field and the signal wave that impinge on the array will hence be of planar character. Furthermore, the signal is assumed to be of narrowband character. This means that the signal is assumed to be present only in a narrow range of frequencies. The signal value at time t in some reference point is denoted as $x(t)$. If nothing else is mentioned the reference point will be assumed to be at the location of the first hydrophone. As

before the difference in arrival times between sensor 1 and sensor n is denoted τ_n. By this notation we are able to define the output of sensor k as in equation (7.1).

$$y_n(t) = h_n(t) * x(t - \tau_n) + \epsilon_n \tag{7.1}$$

where ϵ_k is some noise and $h_n(t)$ is the impulse response of sensor n. Convolutions are in general complicated to work with and therefore it is often more suitable to work in the frequency domain. This can be achieved by applying the Fourier transform defined in equation (7.2)

$$X(\omega) = \int_{-\infty}^{\infty} x(t)e^{-i\omega t}dt \tag{7.2}$$

where ω is the frequency of interest. Using general properties of the Fourier transform, the output of sensor k can be rewritten, see equation (7.3).

$$Y_n(\omega) = H_n(\omega)X(\omega)e^{-i\omega\tau_n} + E_n(\omega) \tag{7.3}$$

From equation (7.3) it is possible to formulate the time domain signal as in (7.4).

$$y_n(t) = H_n(\omega)e^{-i\omega\tau}x(t) + e_n(t) \tag{7.4}$$

Next, in equation (7.5), we introduce the so-called array manifold vector:

$$\boldsymbol{a}(\theta) = \left[H_1(\omega)e^{-i\omega\tau_1} \dots H_N(\omega)e^{-i\omega\tau_N}\right]^T \tag{7.5}$$

Now by making the assumption that each sensor in the array are identical, meaning that an identical signal intercepted at different hydrophones will yield the exact same output, we can redefine $H(\omega)x(t)$ as $x(t)$. Setting the first hydrophone as the reference point ($\tau_1 = 0$), the array manifold vector can be simplified as in equation (7.6)

$$\boldsymbol{a}(\theta) = \left[1 \quad e^{-i\omega\tau_2} \dots e^{-i\omega\tau_N}\right]^T \tag{7.6}$$

The redefined array manifold vector allows us to write the output $\boldsymbol{y}(t)$ for all N sensors in vector form, see equation (7.7):

$$\boldsymbol{y}(t) = \boldsymbol{a}(\theta)x(t) + \boldsymbol{e}(t) \tag{7.7}$$

where

$$\boldsymbol{y}(t) = [y_1(t) \dots y_N(t)]^T \quad and \quad \boldsymbol{e}(t) = [e_1(t) \dots e_N(t)]^T$$

From equation (7.6) it is clear that the array manifold vector depends on the DOA or angle θ due to the dependence on τ_n, see figure 7.1. From figure 7.1, the delay τ_n can be expressed as a function of θ, see equation 7.8 below.

$$\tau_n = (n-1)\frac{d \cdot sin(\theta)}{c} \quad \text{for} \quad n = 2, 3, ...N \tag{7.8}$$

where c is the medium propagation speed. With (7.8) all components of the array manifold vector (7.6) have been explicitly expressed and we can easily extend the ULA model to include more sources as in (7.9).

$$\boldsymbol{y}(t) = [\boldsymbol{a}(\theta_1) \dots \boldsymbol{a}(\theta_M)] \begin{bmatrix} x_1(t) \\ \vdots \\ x_M(t) \end{bmatrix} + \boldsymbol{e}(t) \tag{7.9}$$

In equation (7.9) θ_m is the DOA of the mth source and $x_m(t)$ is the signal corresponding to the mth source. In the multiple sources situation, the output is a vector where each element is the sum of the signals received from all sources by one hydrophone.

There are some limitations to the ULA that deserves to be mentioned at this point. The first restriction is that the DOA, θ, is limited to $[-90^\circ\ 90^\circ]$. This is due to that two sources at locations symmetric with respect to the array line yield identical sets of delays and hence cannot be distinguished from one another. The second important limitation is that the sampling frequency of f should be at least two times the frequency of the input signal ω. If this does not hold the model will display aliasing effects in accordance to the Shannon Sampling theorem, see mathematical formulation in equation (7.10), (Stoica and Moses 2005 p. 285).

$$f \geqslant 2\omega \tag{7.10}$$

7.2 Delay-and-sum Beamformer

Using the setting described in section 7.1 some intuition for the delay-and-sum beamforming method is provided below. The idea is to use filter methods and try to enhance and attenuate the energy from each direction in order to obtain a beampattern (see figure 7.2 for some immediate intuition). In equation (7.11) the output signal is filtered:

$$\boldsymbol{y}_F(t) = \boldsymbol{h}^T \boldsymbol{y}(t) \tag{7.11}$$

where $\boldsymbol{h}$ is some filter to be derived. It is easier to get insight into the filter selection, if the noise free case is considered, see (7.12).

$$\boldsymbol{y}_F(t) = \left[\boldsymbol{h}^T \boldsymbol{a}(\theta)\right] x(t) \tag{7.12}$$

Equation (7.12) is obtained by combining equation (7.7) and equation (7.11). In order for the filter to work well it is natural to impose the following two conditions:

1. The filter $\boldsymbol{h}$ passes undistorted the signals with the true DOA, θ
2. The filter $\boldsymbol{h}$ attenuates all the other DOAs different from θ as much as possible

The power of the spatially filtered signal can be defined as the mean over the energy as in equation (7.13):

$$\mathbb{E}\{|\boldsymbol{y}_F(t)|^2\} = \boldsymbol{h}^T \boldsymbol{R} \boldsymbol{h} \tag{7.13}$$

where $\boldsymbol{R}$ is the covariance matrix of the signal defined as:

$$\boldsymbol{R} = \mathbb{E}\left\{\boldsymbol{y}(t)\boldsymbol{y}(t)^T\right\} \tag{7.14}$$

In view of equation (7.12) the first condition of the filter design problem can be formulated as:

$$\boldsymbol{h}^T \boldsymbol{a}(\theta) = 1 \tag{7.15}$$

The relation in equation (7.16) is also worth to have in mind for the ULA case, where the array manifold vector $\boldsymbol{a}(\theta)$ is normalised:

$$\boldsymbol{a}^T(\theta)\boldsymbol{a}(\theta) = N \tag{7.16}$$

Considering our design criteria and equation (7.15) the design problem can be formulated as an optimisation with boundary conditions, see equation (7.17)

$$\min_h \boldsymbol{h}^T\boldsymbol{h} \quad subject\ to \quad \boldsymbol{h}^T\boldsymbol{a}(\theta) = 1 \tag{7.17}$$

The design problem have the solution (7.18) and the derivation of this solution can be found in (Stoica and Moses 2005, chapter 6).

$$\boldsymbol{h} = \frac{\boldsymbol{a}(\theta)}{\boldsymbol{a}^T(\theta)\boldsymbol{a}(\theta)} \tag{7.18}$$

From equation (7.16) the solution of the design problem reduces to:

$$h = \frac{\boldsymbol{a}(\theta)}{N} \tag{7.19}$$

Inserting the designed filter into equation 7.13 yields

$$\mathbb{E}\{|y_F(t)|^2\} = \frac{\boldsymbol{a}^T\boldsymbol{R}\boldsymbol{a}}{N^2} \tag{7.20}$$

The theoretical covariance matrix $\boldsymbol{R}$ cannot be exactly determined from a finite sample and is therefore estimated as (7.21):

$$\hat{\boldsymbol{R}} = \frac{1}{N}\sum_{t=1}^{N}\boldsymbol{y}(t)\boldsymbol{y}(t)^T \tag{7.21}$$

Where N denotes the total number of observations. The beamforming DOA estimates are finally given by the number of sources highest peaks of the function (7.22).

$$DOA = \boldsymbol{a}(\theta)^T\hat{\boldsymbol{R}}\boldsymbol{a}(\theta) \tag{7.22}$$

Note that we have removed the denominator N^2 since it is a constant and does not change the location of the optimum, only the scale.

Another way to view the delay-and-sum beamformer is to realise that when it is tuned to the true angle θ it will delay the signal at each hydrophone to exactly match up in time. Therefore in the noise free case each hydrophone would record the same signal. In that case, when summing over all hydrophones the sum would become much larger due to constructive interference compared to when looking at any angle different from θ.

In figure 7.2 an example of a beampattern from the beamformer described above is shown. To generate the beampattern a uniform linear array with N=11 sensors have been used. The data have been simulated with some normally distributed noise.

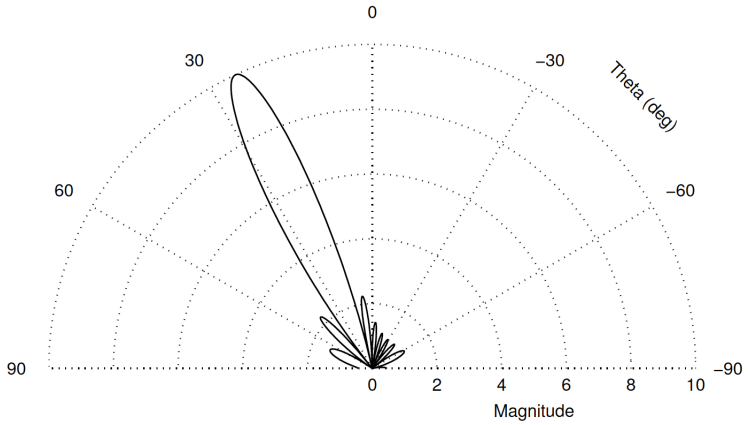

Figure 7.2: *Output of a delay-and-sum beamformer from a uniform linear array with a simulated signal with some normally distributed noise. Source: Stoica and Moses 2005*

7.3 Main lobe and side lobes

One major consideration of any beamforming operation is the presence and relation between main and side lobes. In short the main lobe (or beam) in a beampattern is the peak where the energy of the radiation reaches its maximum, which in figure 7.2 corresponds to the peak around 25^o. The side lobes are basically all the other peaks surrounding the main lobe. The theory behind side lobes and how to optimise over the relation between main and side lobes is extensively researched in the literature. However, it is considered out of scope to, from a theoretical point of view, exhaustively elaborate on the topic in this thesis. Instead the aim of this section is to make the reader aware of the existence and illustrate what aspects affect the relation. Below, three examples of factors which impacts the beampattern are discussed. The list of three factors is non exhaustive and its primary purpose is illustrative. Additional theory on beamforming and the resolution of beampatterns can be found in for example (Liu and Weiss 2010) and (Van Trees 2004)

In figure 7.3, a beampattern is provided in log_{10} scale to make the side lobes more apparent. From studying the figure there is no problem to identify the main beam and the corresponding DOA, marked by a red star. The signal has been simulated with what is being referenced to as a perfect sine, what is meant by this is that the sine wave registered by the hydrophone is noise free. The reader is advised to note that θ here denotes the angle to the x-axis compared to before, where it denoted the angle to the normal of the array. Figure 7.3 is used as a reference to figures 7.4 a), b) and c) to show that the side lobes are not static.

In figure 7.4 a), θ have been reduced making the wave impinge the array more from the side. This causes the beampattern resolution to decrease and it is no longer evident which of the lobes that is the main lobe. Hence, DOA estimation with the delay-and-sum beamformer becomes increasingly difficult as θ approaches the x-axis. There are methods to design other spatial filters to enhance resolution even as θ approaches the x-axis. To enhance resolution, one could also consider mechanical changes, for example moving the array or a different array aperture.

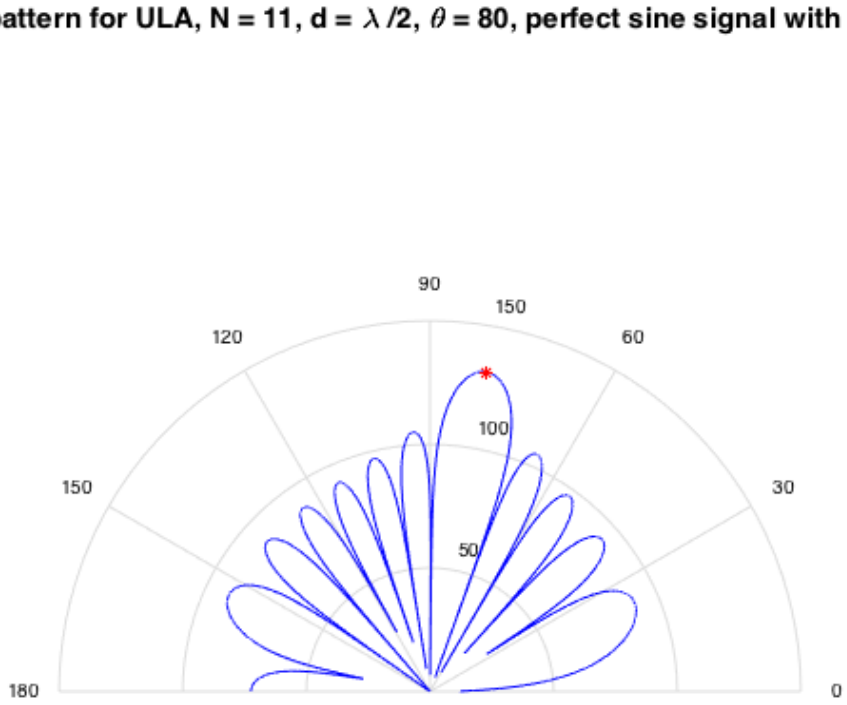

Figure 7.3: *Beampattern, red star marks true DOA. Generated from ULA with N=11 hydrophones with spacing* $\frac{\lambda}{2}$*, energy levels are calculated as* $10 \cdot log_{10}(|\boldsymbol{a}^T(\theta)\boldsymbol{R}\boldsymbol{a}(\theta)|^2)$*. Signal is a noise free (perfect) sine wave with* $\omega = 100$*.*

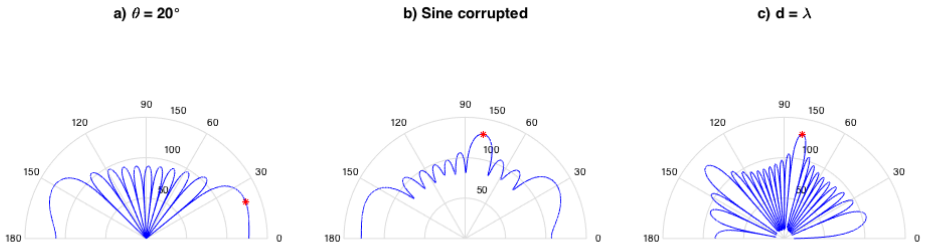

Figure 7.4: *Beampatterns for ULA with* $N = 11$ *hydrophones, red star marks true DOA, energy levels are calculated as* $10 \cdot log_{10}(|\boldsymbol{a}(\theta)^T\boldsymbol{R}\boldsymbol{a}(\theta)|^2)$*. a) Data simulated from perfect sine with* $\omega = 100$ *Hz,* $\theta = 20^o$ $d = \frac{\lambda}{2}$ *b)Data simulated from two perfect sines with* $\omega = 100$ *and* 500 *Hz but only* $\omega = 100$ *Hz searched for,* $\theta = 80^o$ *and* $d = \frac{\lambda}{2}$ *c) Data simulated from perfect sine with* $\omega = 100$ *Hz,* $\theta = 80^o$ *and* $d = \lambda$*.*

On the other hand, in figure 7.4 b), the sine is no longer perfect but contain one more frequency than the one searched for. From the figure, it is evident that this causes the overall energy levels to increase, but it is still possible to identify the main lobe. In the case with only two frequencies the problem could easily be corrected by including the extra frequency and summing over the two beampatterns.

Finally, figure 7.4 c) shows a beampattern where the distance between the hydrophones is changed from the optimal $\frac{\lambda}{2}$ to λ. This introduces a concept called aliasing (Christensen and Hald 2004) and causes the side lobes to multiply. In the

case of aliasing the side lobes are usually called grating lobes. Grating lobes can be particularly troublesome since the main lobe becomes tighter, and designing automatic algorithms to find the main lobe risks identifying one of the side lobes instead.

7.4 Problem Formulation

Using the delay-and-sum beamforming tools described in section 7.2, it is possible to derive a method for AEL using continuous signals from the sound of a powerboat. The idea builds upon that the energy measure defined by equation (7.22) is maximised by the true hydrophone positions. Since, for a given set of hydrophone positions, the theoretical energy for that set of positions is known, it can be used as a criteria for optimisation. The objective function is defined in equation (7.23):

$$\underset{\boldsymbol{p}_2,\boldsymbol{p}_3\ldots,\boldsymbol{p}_N}{\text{maximise}} \quad \sum_{m=1}^{M} |\boldsymbol{a}_m^T(\boldsymbol{P})\boldsymbol{R}\boldsymbol{a}_m(\boldsymbol{P})|^2 \tag{7.23}$$

where, $m = 1, 2, ...M$ runs over each send location and

$$\boldsymbol{a}_m = \begin{bmatrix} 1 & e^{-i\omega\tau_{2m}(\boldsymbol{p}_2)} & \ldots & e^{-i\omega\tau_{Nm}(\boldsymbol{p}_N)} \end{bmatrix}^T$$

The hydrophone positions are again denoted as $\boldsymbol{P} = [\boldsymbol{p}_2, \boldsymbol{p}_3, ...\boldsymbol{p}_N]$ and enters through the calculation of τ defined in equation (7.8) and $\boldsymbol{R}$ is defined as in (7.21). To be able to apply the MatLab optimisation toolbox, the optimisation problem is reformulated as a minimisation as in (7.24).

$$\underset{\boldsymbol{p}_2,\boldsymbol{p}_3\ldots,\boldsymbol{p}_N}{\text{minimise}} \quad -\sum_{m=1}^{M} |\boldsymbol{a}_m^T(\boldsymbol{P})\boldsymbol{R}\boldsymbol{a}_m(\boldsymbol{P})|^2 \tag{7.24}$$

Without loss of generality, the minimisation can be adapted to include more than one frequency as in (7.25) where the frequencies of interest are denoted $\omega_l, \quad [l = 1, 2, \ldots L]$ and L denotes the number of frequencies. By adding more frequencies the narrowband assumption in section 7.1 becomes less strict as more frequencies are added.

$$\underset{\boldsymbol{p}_2,\boldsymbol{p}_3\ldots,\boldsymbol{p}_N}{\text{minimise}} \quad -\sum_{l=1}^{L}\sum_{m=1}^{M} |\boldsymbol{a}_m(\omega_l, \boldsymbol{P})^T\boldsymbol{R}\boldsymbol{a}_m(\omega_l, \boldsymbol{P})|^2 \tag{7.25}$$

7.4.1 Relaxation of far field assumption

The optimisation algorithm described above need some adjustment before being feasible in our real world application of estimating the array elements. The reason is that the classical assumption of far field source location, and its implication of planar waves, is not feasible since the boat drives to close to the array. Theoretically it would be possible to drive the boat further from the array and use the method described above, but in practice this would probably not work since the signal-to-noise ratio, SNR, would be significantly lower.

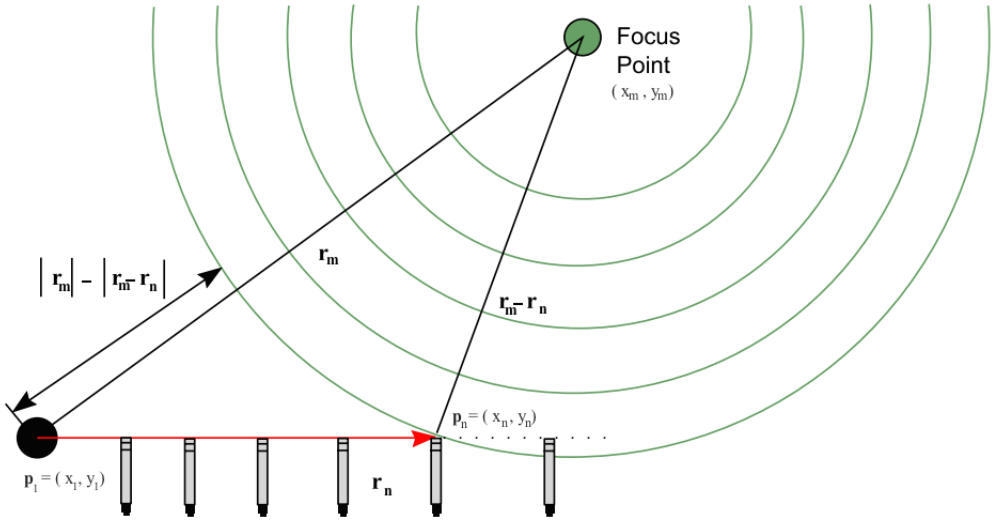

Figure 7.5: *Spherical wave geometry in the single source case. To calculate τ in this setting is the same as subtracting the difference in euclidean distance from the reference point to each hydrophone.*

To correct for the planar wave assumption we need to adapt our calculations of the time delays, τ_{nm}, for each send location to a slightly more complex geometry. The difference is evident from figure 7.5. Using the notation introduced in figure 7.5 it is evident that τ_{nm} can be expressed as in equation (7.26):

$$\tau_{nm} = \frac{|r_m| - |r_m - r_n|}{c} \tag{7.26}$$

where, $|r_m|$ and $|r_m - r_n|$ are calculated as in (7.27) and (7.28)

$$|r_m| = \sqrt{(x_m - x_1)^2 + (y_m - y_1)^2} \tag{7.27}$$

$$|r_m - r_n| = \sqrt{(x_m - x_n)^2 + (y_m - y_n)^2} \tag{7.28}$$

Equipped with this updated calculation of τ_{nm} it is possible to use the delay-and-sum beamformer for a near field source by plugging (7.26) into the equation of the array manifold vector (7.7) (Christensen and Hald 2004). By the same argument the optimisation algorithm in (7.24) can be updated for a near field source by calculating τ_{nm} as (7.26). However, the time complexity will slightly increase since the distance to each send location now needs to be calculated at each function evaluation performed during the optimisation.

7.4.2 Frequency domain covariance matrix

One adaptation of the algorithm that could be advantageous is to calculate the covariance matrix in the frequency domain. There are two main reasons for why this could improve the performance. Firstly, by computing the covariance matrix in the frequency domain only the information for that frequency is included, hence resolution problems, such in figure 7.4 b) would become less significant. Furthermore, in the frequency domain it is also possible to control the size of the frequency bins to for example $1, 5, 10,$ or 100 Hz per bin. By making the bins larger in the

transformation the main lobe would smear out, which could be beneficial since the sensitivity of the optimisation (7.24) to the initial guess could decrease as the likelihood of being close to the main lobe gets larger.

To calculate $\boldsymbol{R}$ in the frequency domain, the Fourier transform is applied using definition (7.2). The mathematical representation becomes as in equation (7.29)

$$\boldsymbol{R}(w) = \boldsymbol{Y}(w) * \boldsymbol{Y}(w)^T \tag{7.29}$$

In (7.29) the $\boldsymbol{Y}(w)$ denotes a N x 1 vector of values from the Fourier transform corresponding to the frequency w.

Powerboat Data

In this chapter, the data used in the final beamforming calibration method is presented. Data has been provided by FOI from a conducted experiment in May 2016. In the experiment, a powerboat drove close by two arrays for 20 minutes. The GPS trace of the boat and the sound intercepted at both arrays were recorded, as in the experiment using pings. The sample rate of the boat-mounted GPS was 1 Hz and the sample rate of the hydrophones were 30 kHz. The experiment took place between 14:50:00-15:09:59. FOI has also provided a data set from a separate experiment where 5 minutes of background noise was recorded at both Pass1 and Pass2.

8.1 Boat-mounted GPS data

In the GPS trace, there are 19 missing data points in the time interval 14:52:00 - 14:53:00. Instead of interpolating between these points the data has been truncated from 14:55:00-15:04:59. The total of 10 minutes data are also deemed to be sufficient for the optimisation to converge in the beamformer algorithm. As shown in figure 8.1, the chosen time segment gives more than one lap around both arrays and the boat has a fairly constant speed at 4.3 m/s.

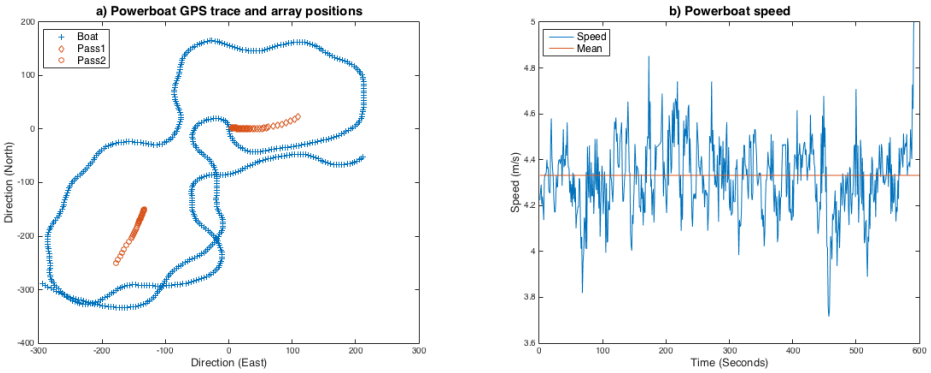

Figure 8.1: *a) The GPS trace from the powerboat taken from time segment 14:55:00-15:04:59 and the estimated array positions from AELUP. b) The boat speed from time segment 14:55:00-15:04:59 and its mean value of 4.36 m/s.*

8.2 Hydrophone recordings

In Pass1, there were 3 dead channels, hydrophones 15-17, resulting in 53 hydrophones to position. In Pass2, there was 1 dead channel, hydrophone 6, resulting in 55 hy-

drophones to position. In figure 8.2, a sample of a time series is shown from 0.2 seconds of data in Pass1. In this time sample it is clear that the powerboat is located closer to hydrophone 53 than hydrophone 1 due to the higher energy in hydrophone 53. In the beamformer algorithm used for the AEL, it is important that:

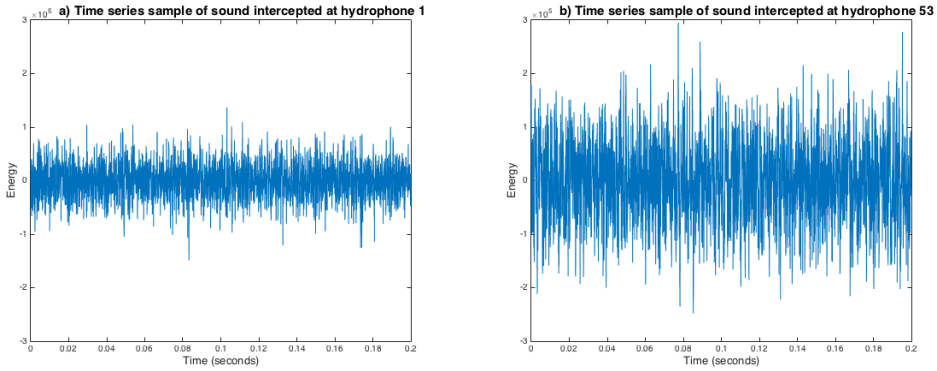

Figure 8.2: *Sample of 0.2 seconds data intercepted at hydrophone 1 and hydrophone 53 in Pass1. In selected time segment the boat is closer to hydrophone 53 resulting in higher energy. The mean has been subtracted from the time-series.*

1. The data is stationary due to estimation of covariance matrix
2. To know what frequencies the powerboat generates

To conclude when the data is stationary, we inspect the spectrogram that shows how the frequencies of a signal change over time. From figure 8.3 a), it is clear that the data is fairly stationary in a sample size of 1 second data, 30.000 data points. To obtain the spectrogram the MatLab function *spectrogram* in the Signal Processing Toolbox were used.

The spectrogram can also be used to distinguish frequencies generated by the powerboat from frequencies in the background noise. By summing spectrograms over 10 minutes of data with FFT window length of 30.000 data points and no overlap, it is fairly clear which frequencies are of interest. The sum of spectrograms were computed for Pass1, Pass2, and the background noise. The spectrogram function apply the FFT-algorithm where the bin resolution can be specified. In the analysis several bin resolutions were tested to identify significant peaks in both the noise and powerboat sound. In figure 8.4, a bin resolution of 10 Hz/bin were used. Note that the scale of the spectrograms are in log-scale and that 100 Hz seem to be a dominating frequency generated by the powerboat for both Pass1 and Pass2. In the beamform calibration method, several frequencies are summed and therefore it might be important to consider the signal-to-noise ratio. The SNR is shown in figure 8.3 b) and SNR is similar for Pass1 and Pass2. A SNR value less than zero means that the noise is dominating the signal from the powerboat. This is only the case for Pass2 in frequency band 10-20 Hz.

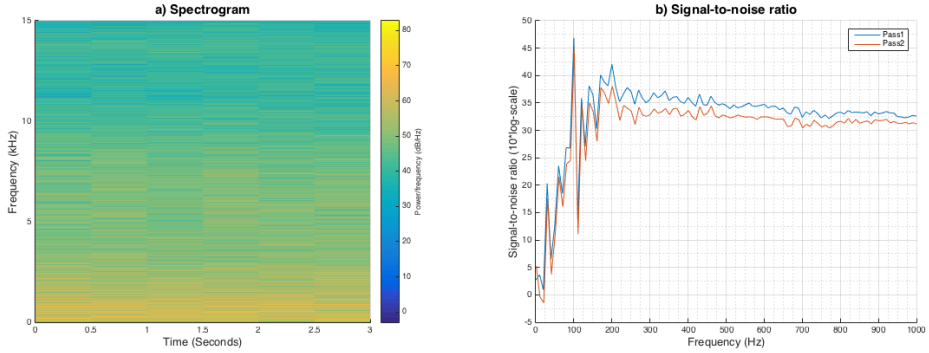

Figure 8.3: *a) The spectrogram of 3 seconds of data using a window length of 15000 data points, 1 Hz/bin resolution and no overlap. b) The signal-to-noise ratio is maximised around 100 Hz for both pass1 and pass2 and low for frequencies below 50 Hz. The fast-fourier-transform resolution is set to 10 Hz/bin to distinguish main peaks.*

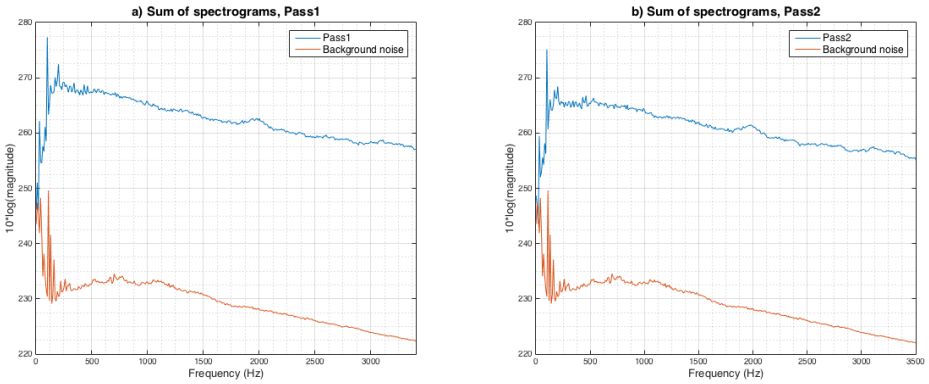

Figure 8.4: *The sum of spectrograms of hydrophones 1-39 from time segment 14:55:00-15:04:59 using windows of 1 second stationary data and no overlap. The number of points used in the fast-fourier-transform is set to 3000 samples yielding a resolution of 10 Hz/bin. The sum of spectrograms of the background noise is computed from 10 minutes of data when the boat is not present.*

Simulation

Working with large data sets and complex algorithms, it's in general a good idea to break down the problem into smaller parts. This was done by building a step-by-step simulation of the real world problem in MatLab. Throughout the working process of this thesis, the complexity of the simulation have increased. For instance, in an early version the simulation was two-dimensional and the sources generated planar waves. In later versions, it was extended to three dimensions and spherical waves. The goal with the simulation was to let the AEL objective function, derived in section 7.4, achieve convergence to the true hydrophone positions. Another reason for simulating is to evaluate the parameters of the model and to understand their individual impact on the result. The objective function is proven to perform well in a simulated environment.

9.1 Method

Two signals were generated to evaluate the beamforming calibration method. The first signal was a pure sine wave generated at 100 Hz, referred to as the *narrowband signal*. The second signal was an attempt to mimic the powerboat sound in the frequency band 0-340 Hz, referred to as the *broadband signal*. This was done by identifying high frequency peaks from the sum of spectrogram plots, see figure 8.4, and add the background noise that was modelled in the frequency band 0-340 Hz. The spectrograms of the signals are shown in figure 9.1.

The real GPS data, see figure 8.1, was set as the signal sources, 600 data points, and the estimated positions from the AELUP were set to the *true positions* of the hydrophones from where the signals were sampled. A perfect result in the simulation is therefore when the algorithm converge to the estimated AELUP positions, referred to as the *true positions*.

The AEL objective function, (7.24), was minimised using *fminunc* from the built in MatLab toolbox *Optimization*. *fminunc* finds minimums of unconstrained multivariate functions, using the Quasi-Newton Algorithm. To initialise the optimisation, the objective function is given an initial guess. The guess is set to a perfect linear array, which are the assumed positions by FOI after sinking Pass1 and Pass2. To save computational power, we did not optimise over all 340 frequencies, instead we optimise only over a selection of strong frequencies that are present in the signal. In order to evaluate the results numerically, the error was defined as the average

deviation in euclidean distance for each hydrophone from the assumed true positions:

$$\epsilon = \frac{1}{N} \sum_{k=1}^{N} \|\boldsymbol{p}_{k,est} - \boldsymbol{p}_{k,true}\| \tag{9.1}$$

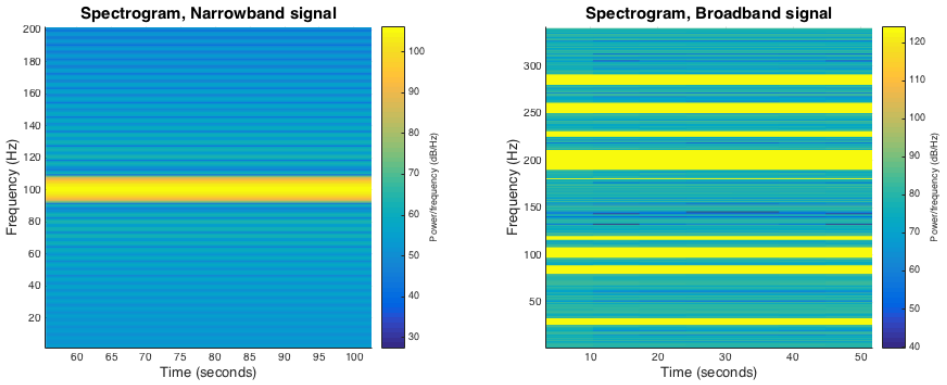

Figure 9.1: *The spectrograms of the simulated narrowband and the broadband signal. The spectrograms show stationary data where the frequency do not change over time. The resolution is set to 8 Hz/bin in FFT for the narrowband signal and 1 Hz/bin for the broadband signal.*

9.2 Simulation with covariance matrix in time domain

In early versions of the simulation, the covariance matrix was estimated in the time domain according to equation (7.21). The beamforming calibration method did not converge to desirable results. Typically, the solution found the correct pattern of the array structure, however drift and compression of the pattern frequently occurred. In all results presented in section 9.2-9.3, the selected optimisation frequencies were set to 100 Hz and 84, 100, 118, 200, 285 Hz for the simulated narrowband and broadband signal, respectively.

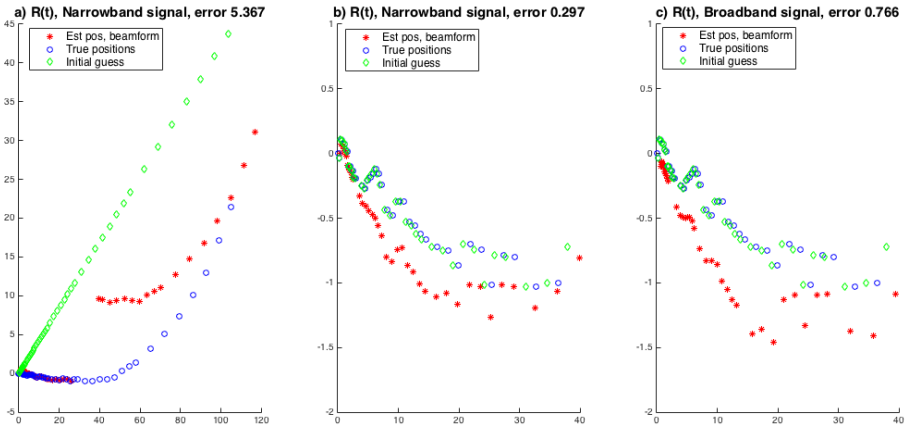

Figure 9.2: *AEL estimation of 53 hydrophones in Pass1, estimating the covariance matrix in the time domain. a) Narrowband signal and initial guess is set to the assumed positions, error 5.367 m. b) Narrowband signal and initial guess is set close to true positions, error 0.297 m. c) Broadband signal and initial guess set close to true positions, error 0.766 m. All plots show the drift behaviour caused by the covariance matrix.*

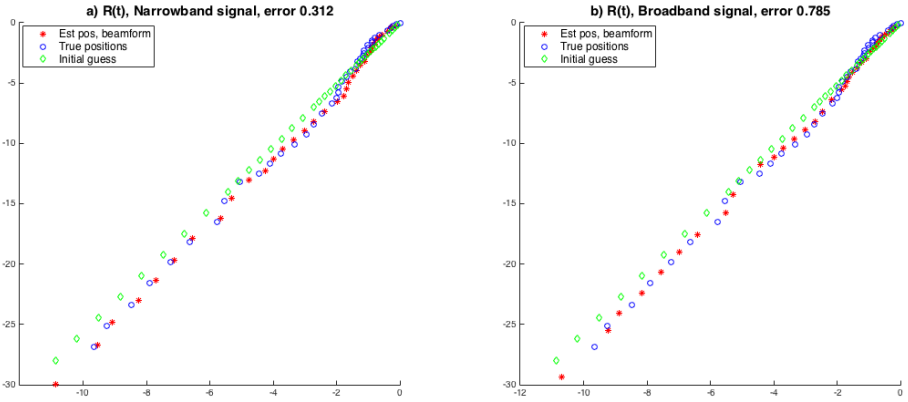

Figure 9.3: *AEL estimation of 55 hydrophones in Pass2, estimating the covariance matrix in the time domain. a) Narrowband signal and initial guess set to assumed positions, error 0.312 m. b) Broadband signal and initial guess set to desired positions, error 0.785 m. Both plots show drift behaviour caused by the covariance matrix.*

9.3 Estimating the covariance matrix in the frequency domain

To deal with the compression and drift, the covariance matrix was estimated in the frequency domain. The intuition is that the time representation is prone to get stuck in a local minimum caused by sidelobes and narrow mainlobe in the beamformer. An advantage with the frequency representation is that it allows for tuning the width of the main lobe in the beamformer by varying the bin resolution in the FFT. Decreasing the bin resolution in the FFT prevents the optimisation to get stuck in local minimums caused by sidelobes. Setting the bin resolution to 3.66 Hz/bin gives the results presented in figures 9.4-9.5. From the results, it is clear that estimating

the covariance matrix in the frequency domain outperform doing so using the time domain representation and that the desirable array positions are not sufficient as initial guess for the optimisation in Pass1.

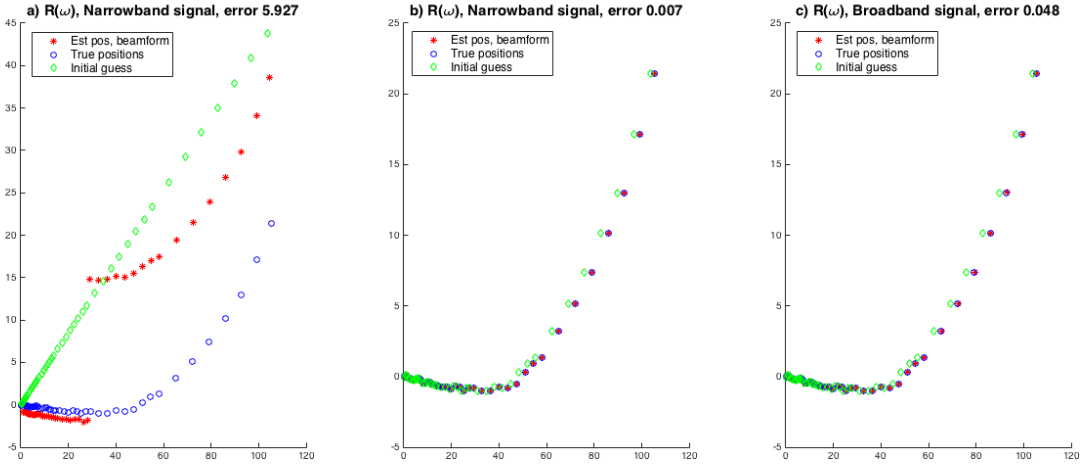

Figure 9.4: *AEL estimation of 53 hydrophones in Pass1, estimating the covariance matrix in frequency domain and bin resolution 3.66 Hz/bin. a) Narrowband signal and initial guess set to assumed positions, error 5.927 m. b) Narrowband signal and initial guess set close to true positions, error 0.007 m. c) Broadband signal and initial guess set close to true positions, error 0.047 m. The error in Pass1 have decreased significantly estimating covariance matrix in frequency domain.*

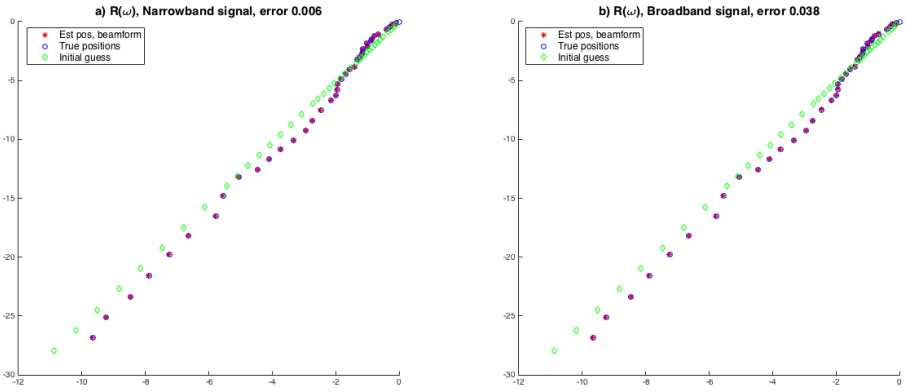

Figure 9.5: *AEL estimation of 55 hydrophones in Pass2, estimating the covariance matrix in frequency domain and bin resolution 3.66 Hz/bin. a) Narrowband signal and initial guess is assumed positions, error 0.006 m. b) Broadband signal and initial guess set to desired positions, error 0.037 m. The error in Pass2 have decreased significantly estimating covariance matrix in frequency domain.*

9.4 Sensitivity analysis

Before switching to real data, a sensitivity analysis was performed. Uncertainties such as acoustic wave reflections on the surface are hard to encapsulate in a simulation but will be further commented on in the discussion chapter. However trying to better understand the effect of the individual parameters will help modelling the

real data set. In table 9.1, a sensitivity analysis is presented. In the analysis, the broadband signal was used and optimisation frequencies set to 100, 200 Hz the first run, row 1, is the reference error. From table 9.1 we can conclude that 600 sources

Sources	FFT Hz/bin	Overlap	Δ GPS	ω	c	ϵ
600	3.66	2192	-	100, 200	1435	0.047
200	3.66	2192	-	100, 200	1435	0.048
100	3.66	2192	-	100, 200	1435	0.065
600	1	0	-	100, 200	1435	0.033
600	60	0	-	100, 200	1435	0.217
600	60	400	-	100, 200	1435	0.068
600	3.66	2192	-	146, 219	1435	0.636
600	3.66	2192	-	146, 200	1435	0.126
600	3.66	2192	-	100, 200	1500	0.856
600	3.66	2192	$\sim \mathcal{U}$(-2,2)	100, 200	1435	0.856
600	3.66	2192	$\sim \mathcal{U}$(-7,7)	100, 200	1435	1.183
600	3.66	2192	+7 m NW	100, 200	1435	0.857

Table 9.1: *The first row is the reference run with an error of 0.047. Setting the FFT resolution to 1 Hz/bin decrease the error and so does introducing overlap in the FFT windows. The model is not robust to noise in the GPS positions nor optimising over weak frequencies.*

seem to be enough data to locate the hydrophones. Increasing the bin resolution and the overlap decrease the error. It seems that optimising over non-present or weak frequencies cause drift and increase the error. The model seem quite sensitive to additive noise in the GPS and propagation speed constant. A final note is that the simulation is not sensitive to optimise over non-design frequencies.

Result, Beamforming Models

In this chapter, the results from the developed beamforming calibration method are presented. All results in this section are from the real data set. To not overwhelm the reader with results, the main focus, in the simulations shown, is on the easier positions in Pass2. When testing the algorithm on real data the model was progressively adapted to become more efficient. For the most effective algorithms the results for Pass1 are also presented.

10.1 First model

A first approach to model Pass2 was to directly apply the final simulation model, here referred to as the first model, and swap the simulated broadband signal to the measured signal. The frequencies applied are the ones most present in the sum of spectrograms in figure 8.4. The results, presented in figure 10.1, show the results for two different bin resolutions. Interestingly, it is noted that when using

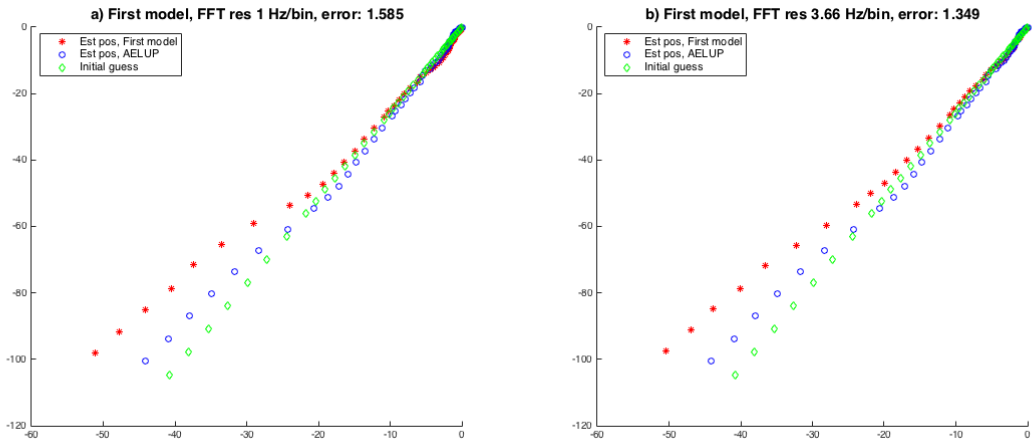

Figure 10.1: *AEL estimation of 55 hydrophones in Pass2 using first model, final simulation model, using two different resolutions in the covariance matrix. The model locates the hydrophone pattern well but there seem to be drift in the converged solution.*

real data the model error decreases when the bin resolution decreases, i.e., each bin becomes larger. This stand in stark contrast to what was experienced in simulated environments where the opposite was true. Furthermore, from visual inspection it is noted that there are significant differences between the AELUP algorithm and the first model. Therefore, the results can be seen as promising, because the estimated positions moves in the right direction, but not good enough.

10.2 Nested model with design frequencies

During the simulations, it was not obvious that the design frequencies were essential for the algorithm to converge to the correct positions. However, when the head on approach of switching from simulated data to measured data worked poorly, see figures 10.1 a) and b), it seemed natural to take the design frequencies into account. This was done by dividing the array into nests according to the design frequencies.

In the following models, the design frequencies presented in table 10.1 will be used for nest-by-nest optimisation. The selected frequencies were chosen after several trial runs. In figures 10.3 a)-f), the results are displayed for each uniform linear array nest in Pass2. The definition of the nests is found in table 3.1. In the AEL estimates the dead channels have been removed. In figure 10.2 the results from all nests are shown in the same figure together with the mean value of the estimated positions that occur in several nests. In figure 10.3, the result of each nest is shown separately.

The results in figure 10.2 are clearly better than in figure 10.1, this is evident from visual inspection. The error is also smaller, 1.22, for the mean of the estimations compared to the first model with error of 1.34. However, there are still some unwanted drift in the solution.

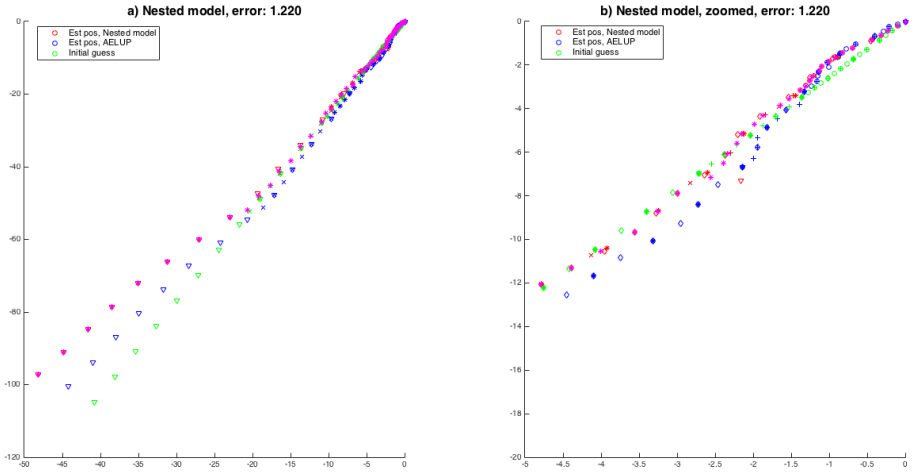

Figure 10.2: *AEL using Nested model in Pass2 with frequencies close to the design frequency, see table 10.1. Each nest is marked with their own marker, the magenta coloured markers denote the mean estimated position. There are still drift in the beamforming algorithm solution. Plot b) is zoomed a) to give better resolution around origo.*

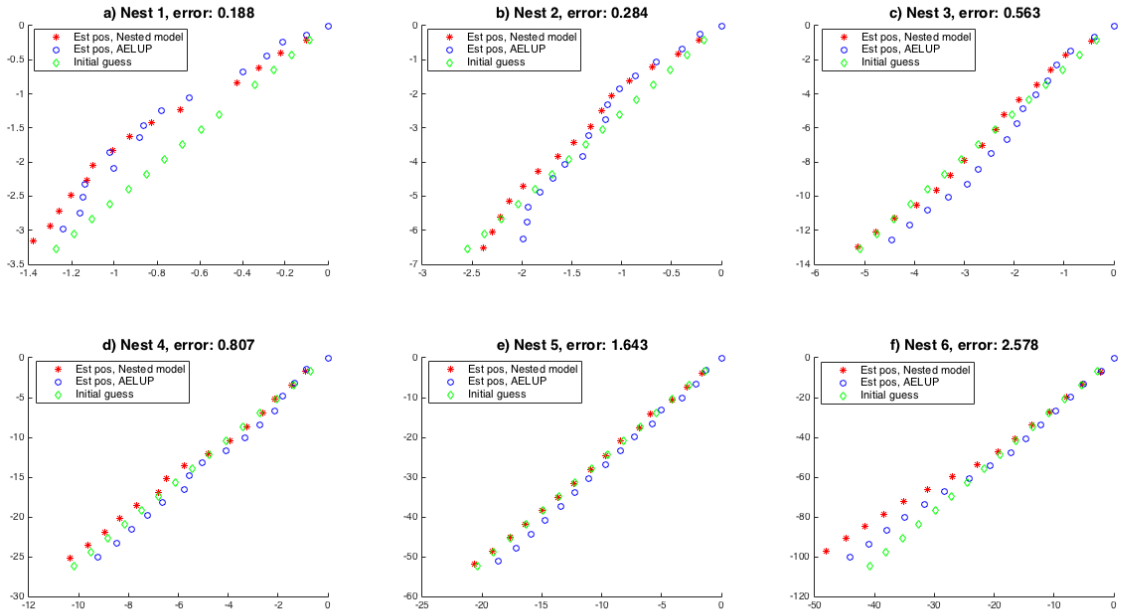

Figure 10.3: *AEL of nest-by-nest method in Pass2 using frequencies close to the design frequency, see table 10.1. The positioning error, 1.22, improves compared to the first model and there are less drift behaviour.*

Nest	Optimising frequencies ω
1	2900, 3000, 3075, 3150, 3200, 3300
2	1430, 1480, 1530, 1580, 1630, 1730
3	565, 665, 710, 765, 815, 865
4	180, 280, 330, 380, 430, 480
5	141, 156, 191, 216, 241, 291
6	80, 104, 144, 172, 355, 445

Table 10.1: *The nest-by-nest frequencies that the objective function minimise over.*

10.3 Two step model

In section 10.2, it was shown that using design frequencies significantly improved the results. Design frequencies could be problematic since they do not necessarily coincide with frequencies in the powerboat data. By studying the sum of spectrograms, figure 8.4, it is clear that the sound the powerboat generates is relatively weak for higher frequencies. The main problem with using frequencies far from the design frequency is, as discussed in section 7.3, the aliasing effects. Therefore, it could make sense to run the algorithm in two steps for nests with high design frequencies. The reason is that if the algorithm is first run for frequencies close to the design frequency, these estimates are likely to be close to the true hydrophone positions since the risk of ending up in a side lobe is small. The first estimates can then be used as initial guesses for the optimisation but this time with frequencies more present in the powerboat data. Despite a narrower main lobe in the second step the risk of optimising over a side lobe would be less significant as the initial guesses would be much better. The results of the optimisation are displayed in figure 10.4.

From visual inspection of figures 10.4 a) and b) it is evident that the results

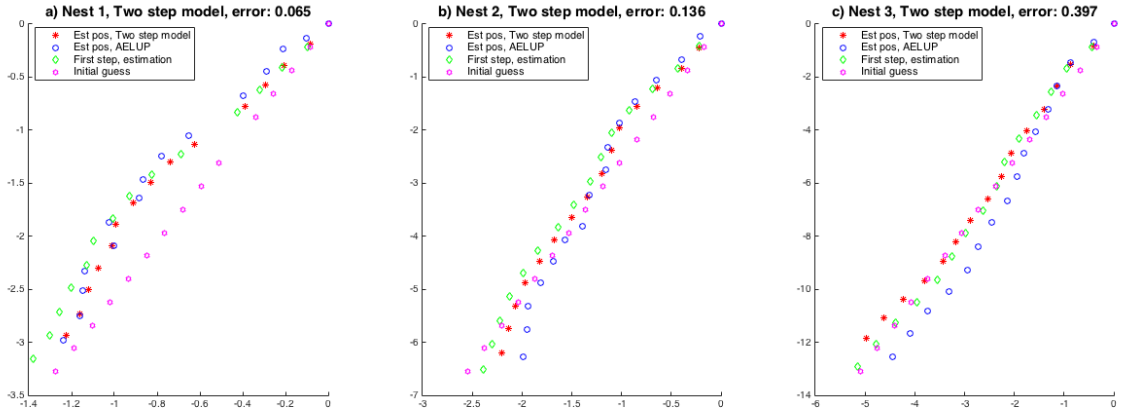

Figure 10.4: *Results for nest 1, 2 and 3 in the two step model. In the first step the same frequencies, as in the nested model form table 10.1, were used. The mean error in nest 1-3 has improved from 0.56 to 0.40.*

improves for the two step model. This is supported by the error measurements, which decrease from 0.19 and 0.28 respectively to 0.065 and 0.14. On the other hand in figure 10.4 c) it is not clear that the two step algorithm improves results. Comparing the green and the red markers it appears as if the red (two step model estimates) sometimes are closer to the estimates from the AELUP, while it at other times is the other way around. Comparing the error it is noted that the result are close but slightly better, 0.56 compared to 0.40, for the two step model.

For the three remaining nests the two-step algorithm was also applied. By the logic of a previous paragraph the potential for improvement with a two step model for these nests is not as great since the powerboat emits high energy waves close to their design frequencies. When trying to run the algorithm with high frequencies the estimates actually turned out further away from the AELUP estimates and hence they were disregarded.

In total, it can be said that for nests were the design frequencies are not obvious in the powerboat data the results are much improved by a two step algorithm.

10.4 Three dimensional model

By recommendation of FOI the third dimension, the ocean depth, was initially not optimised over. There are two reasons for why this simplifying assumption was made. Firstly the time complexity of the proposed algorithm is high, and adding a third dimension increases it further. It is easily realised that the concern is valid, the data files with the measurements are in the size of tens of gigabytes and with the third dimension the optimisation problem to solve becomes a 150+ dimensional non-linear optimisation problem.

Secondly the site of the hydrophone array is known to FOI and the sea depth

should be close to 30 meters and the sea floor should be (more or less) flat in the area. In spite of this, and with the hope of improving the results the algorithms were adapted to include a third dimension. From a theoretical point of view there is no real difference between the two cases and therefore the results are presented straight up in figures 10.5 and 10.6. The model considered for this purpose is referred to as the three dimensional model.

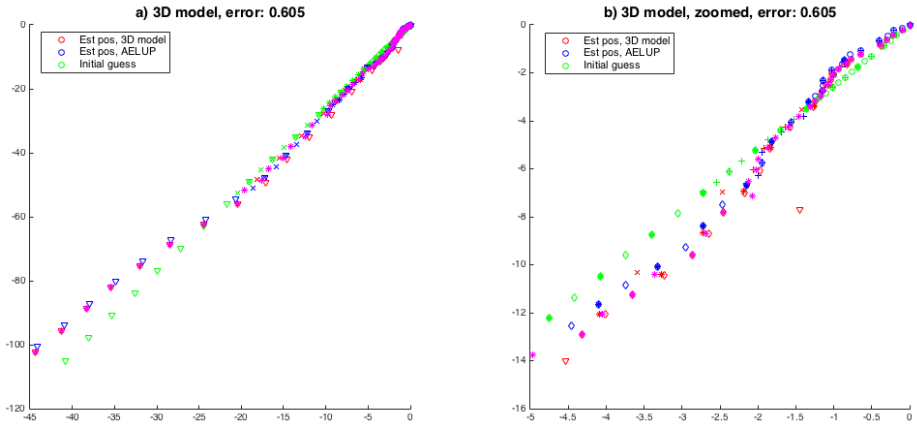

Figure 10.5: *AEL of 55 hydrophones in Pass2 using 3D model, plotted in x,y-plane. The design frequencies from table 10.1 were used. Each nest is marked with their own marker, the magenta coloured markers denote the mean estimated position. The previous drift pattern have disappeared and the total mean error is further decreased to 0.605.*

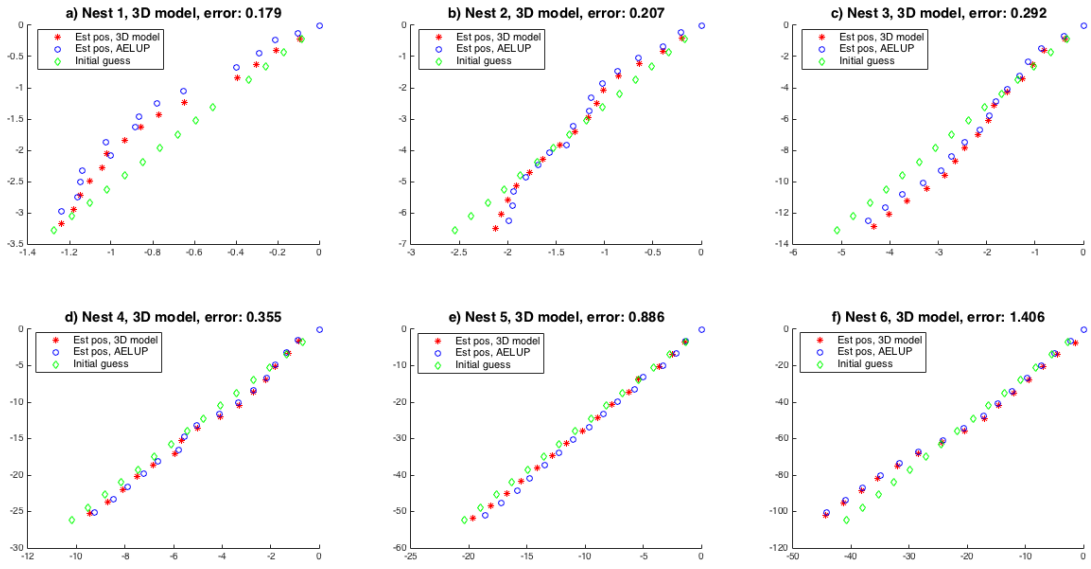

Figure 10.6: *Result from a 3D model on each nest plotted in x,y-plane. The model converges to positions close to the AELUP estimates and there are no longer any drift patterns in the solution.*

The errors reported in figures 10.6 have been calculated as before, that is in two dimensions. This is to maintain the possibility to compare the errors to each other. The errors of the three dimensional model are satisfyingly low both in figures 10.5

and 10.6. For example, by comparing the error of the mean of the estimates in figures 10.2 and 10.5, it falls from 1.22 to 0.61. Furthermore, the error in figure 10.6 c), is also smaller than in the two step algorithm, see figure 10.4. However, for the first and second nest the error is still smaller for the two step algorithm than the three dimensional one.

In table 10.2 the depth and the distance between the hydrophone estimates in the three dimensional model are displayed for each nest. There are several interesting aspects to note. Firstly, by studying the second last column it is seen that the maximum depth difference over the array is a full 9.87 meters. When considering this depth difference one should remember that the corresponding array nest is over 100 meters long implying that this is not a steep inclination. However, it would clearly impair a model which assumes a flat sea floor. Furthermore, it is noted that there are violations to the maximum distances, see table 3.1, but the violations are not in the extreme but generally around a few decimetres. Finally, the reader is encouraged to compare the estimated depths for hydrophones that have been estimated in multiple nests. For example the depth of hydrophone 8 have been estimated in nest 1,2,3 and 4 to respectively z = -0.22, -0.24, -0.39 and -0.24.

N1	z	d	N2	z	d	N3	z	d	N4	z	d	N5	z	d	N6	z	d
1	0.00	0.23	1	0.00	0.46	1	0.00	0.97	1	0.00	1.80	1	0.00	3.84	1	0.00	8.23
2	-0.03	0.23	3	-0.04	0.47	5	-0.21	0.90	8	-0.24	1.86	16	-0.50	3.64	24	-2.52	7.01
3	-0.04	0.24	5	-0.13	0.47	8	-0.39	0.92	16	-0.56	1.87	24	-0.95	3.60	32	-2.38	7.15
4	-0.07	0.24	6	-0.15	0.46	12	-0.59	0.95	20	-0.88	1.89	28	-1.62	3.76	36	-3.51	7.74
5	-0.11	0.47	8	-0.24	0.47	16	-0.81	0.93	24	-1.23	1.86	32	-1.74	3.70	40	-3.91	7.54
6	-0.14	0.23	10	-0.32	0.46	18	-0.98	0.92	26	-1.60	1.85	34	-2.22	3.65	42	-4.57	7.49
7	-0.17	0.23	12	-0.42	0.47	20	-1.06	0.94	28	-1.95	1.85	36	-2.46	3.86	44	-5.43	7.60
8	-0.22	0.23	14	-0.52	0.48	22	-1.18	0.97	30	-2.14	1.84	38	-2.55	3.82	46	-6.23	7.61
9	-0.24	0.23	16	-0.63	0.45	24	-1.38	0.91	32	-2.33	1.74	40	-2.67	3.72	48	-6.68	7.50
10	-0.25	0.24	17	-0.64	0.49	25	-1.59	0.94	33	-2.54	1.82	41	-2.82	3.70	49	-7.38	7.42
11	-0.29	0.22	18	-0.72	0.46	26	-1.83	0.94	34	-2.62	1.83	42	-3.19	3.60	50	-7.51	7.66
12	-0.33	0.24	19	-0.77	0.46	27	-2.05	0.95	35	-2.56	1.75	43	-3.40	3.78	51	-8.62	7.61
13	-0.36	0.23	20	-0.76	0.47	28	-2.17	0.88	36	-2.66	1.83	44	-3.54	3.60	52	-8.82	7.37
14	-0.40	0.24	21	-0.78	0.45	29	-2.22	0.91	37	-2.73	1.80	45	-3.66	3.72	53	-9.36	7.43
15	-0.46	-	22	-0.84	0.48	30	-2.31	0.91	38	-2.79	1.81	46	-4.01	3.65	54	-9.65	7.43
-	-	-	23	-0.95	-	31	-2.48	-	39	-2.87	-	47	-4.23	-	55	-9.87	-

Table 10.2: *Result for Pass 2 in the three dimensional case. First column, Nx, display hydrophones in nest x, second column, z, show the estimated depth (compared to 30 meters below the surface) of the corresponding hydrophone and third column d, shows the distance between two consecutive hydrophones within the same nest.*

10.5 Pass 1

While the results from Pass2 were looking increasingly promising improvements in the results for Pass1 have eluded the authors. Despite fierce testing of models that have converged toward the correct position in Pass2 the results on Pass1 are still disappointing. In this section results that show the difficulties with Pass1 are presented and reasons for the poor convergence are discussed in chapter 11.

10.5.1 Nested Model with Design Frequencies

The results for the same model that was used in section 10.2 for Pass2 are presented for Pass1 in figure 10.7. By visual comparison between figures 10.7 and figure 10.3 it is evident that the algorithm performs much better on Pass1. An attempt to improve the model was tried by using a model similar to the one tried in section

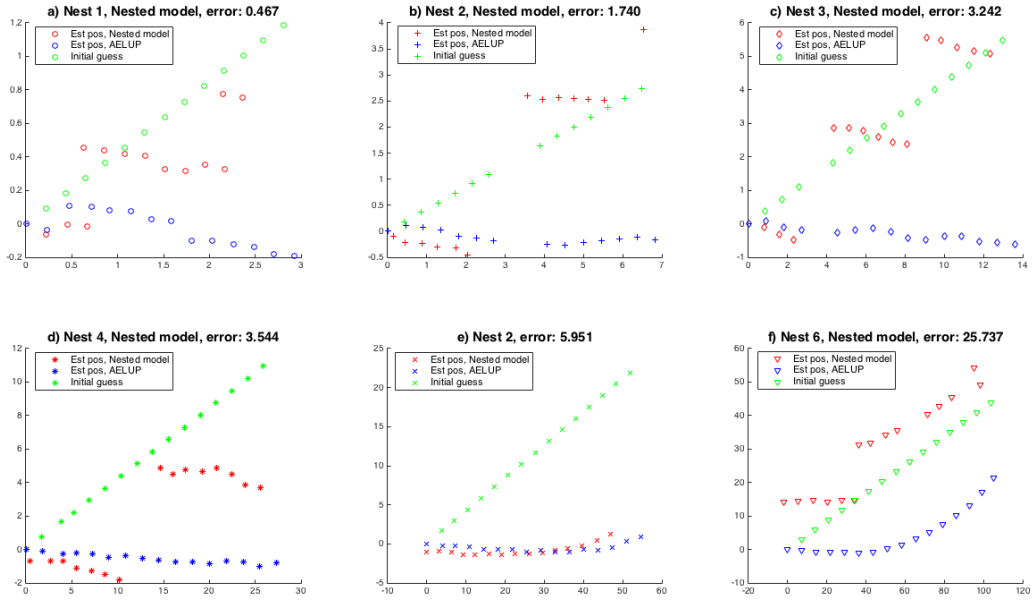

Figure 10.7: *Pass1 nested model with design frequencies. The beamforming calibration method seem to find the pattern of the array well but drift and compression effects occur. The drift and compression cause the error to be significantly larger compared to Pass2.*

10.3. However, no measurable improvement in the results was accomplished by the second step.

10.5.2 Constrained Three Dimensional Model

The model with the lowest error for Pass1 for all nests except the two first was the 3D model described in section 10.4. Naturally an attempt with this model was applied on Pass1, however the results were highly disappointing as the optimisation algorithm converged to depths that were unfeasible. The depths could easily be deemed unfeasible as the distance restrictions were acutely violated.

In an attempt to circumvent this problem a three dimensional constrained model was developed and applied. The model imposes boundary conditions similar to those in section 6 but in three dimensions. In other words the search areas described in figure 6.1 was changed to spheres instead of circles. The method still relied on the beamforming method and apart from the extra boundary conditions the model is the same as in 10.4. The results are displayed in figure 10.8 and table 10.3

Visual inspection and the error sizes show that not even the constrained 3D model manages to locate the hydrophones for Pass1. In table 10.3 the nests and corresponding depth and distance is shown for each hydrophone. Since the results are far from the estimations of the AELUP it is hard to use these estimates for anything. Worth to mention however is that the constrained model seems to enforce the intended distance restrictions, compare to table 3.1. The violations that still occur are either the distance between the first and second hydrophone, which is not optimised over, or because of the dead channels.

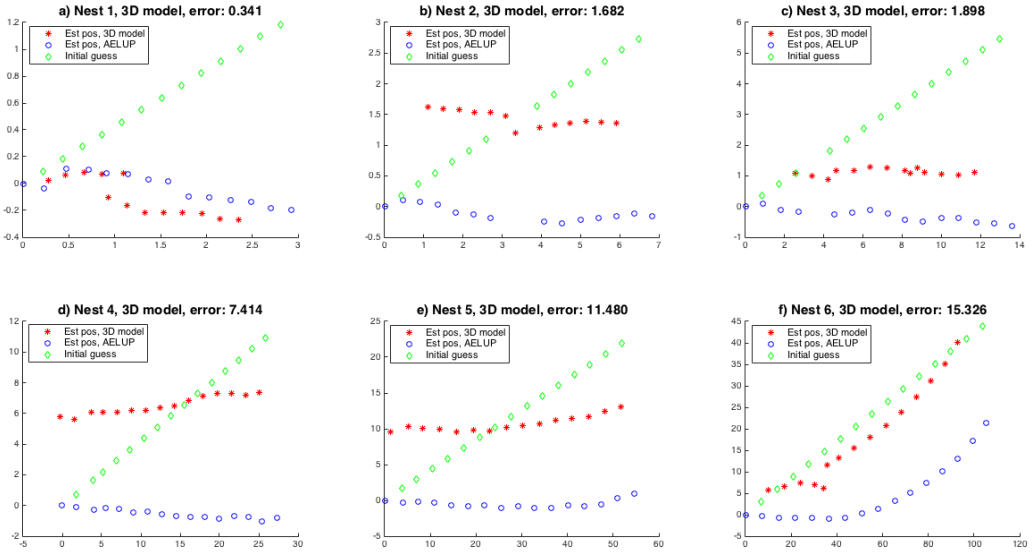

Figure 10.8: *Result from the constrained 3D model on each nest in Pass1. The beamforming calibration method seem to find the array pattern in all nests but severe drift and compression occurs.*

N1	z	d	N2	z	d	N3	z	d	N4	z	d	N5	z	d	N6	z	d
1	0.00	0.29	1	0.00	1.97	1	0.00	2.85	1	0.00	5.94	1	0.00	9.98	1	0.00	12.02
2	0.07	0.19	3	0.06	0.39	5	0.69	0.85	9	-1.42	1.84	15	-2.71	4.01	22	3.09	7.44
3	0.09	0.20	5	0.14	0.40	9	0.81	0.86	15	-1.46	2.29	22	-1.95	3.23	30	5.87	7.45
4	0.12	0.20	7	0.19	0.41	13	0.74	1.86	18	-1.06	1.39	26	-1.77	3.70	34	8.45	7.26
5	0.17	0.24	9	0.23	0.40	16	-1.05	0.88	22	-1.03	1.86	30	-1.38	3.71	38	11.69	5.73
6	0.19	0.25	11	0.22	0.40	18	-1.18	0.88	24	-0.86	1.86	32	-1.46	3.71	40	7.46	7.49
7	0.20	0.22	13	0.31	0.39	20	-1.00	0.89	26	-0.66	1.86	34	-0.81	3.71	42	2.48	7.28
8	0.16	0.20	15	0.18	0.63	22	-0.83	0.89	28	-0.34	1.86	36	-0.42	3.71	44	-2.40	7.43
9	0.19	0.21	16	0.29	0.39	23	-0.75	0.88	30	0.07	1.86	38	0.33	3.70	46	0.08	7.47
10	0.18	0.21	17	0.30	0.40	24	-0.18	0.93	31	0.42	1.86	39	1.09	3.70	47	0.28	7.48
11	0.16	0.21	18	0.34	0.41	25	0.66	0.86	32	0.88	1.86	40	1.76	3.69	48	1.49	7.48
12	0.17	0.21	19	0.36	0.40	26	1.13	0.87	33	1.17	1.86	41	2.65	3.68	49	2.29	7.48
13	0.22	0.21	20	0.41	0.39	27	1.29	0.87	34	1.46	1.85	42	3.31	3.67	50	3.34	7.48
14	0.22	-	21	0.48	-	28	1.39	0.86	35	1.75	1.85	43	3.69	3.65	51	4.57	7.46
-	-	-	-	-	-	29	1.54	-	36	2.21	1.82	44	4.04	3.64	52	4.22	7.45
-	-	-	-	-	-	-	-	-	37	2.47	-	45	4.68	-	53	4.94	-

Table 10.3: *Result for Pass1 in the constrained three dimensional case. First column, Nx, display hydrophones in nest x, second column, z, show the estimated depth (compared to 30 meters below the surface) of the corresponding hydrophone and third column d, shows the distance between two consecutive hydrophones within the same nest.*

10.6 Summary results

In table 10.4 the results from all models presented in this chapter have been summarised. The best fitted model is the three dimensional model for Pass2. No suitable model was found for Pass1 where drift and compression frequently occurred.

	N1	N2	N3	N4	N5	N6	**Mean**
First Model Pass2	0.254	0.237	0.2709	0.535	1.333	3.228	**1.349**
Nested Model Pass2	0.188	0.284	0.563	0.807	1.643	2.578	**1.220**
Nested Model Pass1	0.467	1.740	3.242	3.5437	5.951	25.737	**8.665**
Two-step Model Pass2	0.065	0.136	0.397	0.807	1.643	2.578	**1.067**
3D-Model Pass2	0.179	0.208	0.292	0.355	0.886	1.406	**0.605**
Constrained 3D-Model Pass1	0.341	1.682	1.898	7.414	11.480	15.326	**7.200**

Table 10.4: *Comparison between the results of different beamforming models by their error in meters, see 9.1. The first model is the model with best performance in the simulation, it is calculated as non-nested (simulataneous estimation of all hydrophones). The error of each nest is the corresponding error of that nest. Since the results for Nest 4-6 performed worse for the two step algorithm the results of the Nested model P2 was used instead.*

Discussion

11.1 Calibration of Pass2

The estimated hydrophone positions for Pass2 are, for both the two step model and the three dimensional model, close to the AELUP estimates. It is important to keep in mind that the results of the AELUP algorithm is not considered to be exact, but are themselves estimates and suffer from an unknown error. However, considering that both methods in Pass2 agrees, it is deemed probable that the array performance would increase using either beamform calibration method.

Without an appropriate key, it is difficult to compare the robustness of the results between the three dimensional algorithm and the two-step algorithm. The situation is further complicated by the contradiction in that the sea floor is believed to be flat, while the estimates show a significant inclination. Therefore, it would be recommended to get more accurate measurements of the sea floor at the array sites. Potentially, there could already exist sufficiently detailed ocean charts to make the call if the estimated depths are feasible. However, the authors are not able to consult such charts since the array locations are classified information.

When comparing the positions, both in two and three dimensions, of hydrophones which occur in multiple nests, some differences in the estimates are evident. Generally, the differences are not huge and the mean value is usually close to the current model estimates. In total, except for a few exceptions the differences are deemed within the margin of error.

In total, the results for Pass2 must be considered a success. Before starting this project, the problem was recognised to be hard. In general the problem of estimating, or even worse, calibrating arrays from continuous signals, such as the powerboat sound, is a recognised difficult problem. Furthermore, the conditions in the ocean, discussed further in section 11.2.1, are particularly troublesome with high noise levels.

11.2 Calibration of Pass1

The discussion of why the performance of the algorithm is worse for Pass1 is perhaps more interesting than the discussion for Pass2. Already in the simulations it was shown that Pass1 would be more troublesome. The possible sources of error that

could cause the poor performance are discussed in the next section.

11.2.1 Sources of error

Initial Guess in the optimisation

One obvious reason, as shown in the simulation, is that the initial guess for the optimisation is too far off the true positions of the array. In this thesis it was chosen not to present any figures of the real data with better initial guesses, since in practice the only feasible guess is the nominal array positions. Setting a different initial guess would therefore be a sort of cheating. However, even if the initial guess was set close to the AELUP estimates the algorithm did not converge to those estimates. It was noted that the objective function in the minimisation had higher values in the AELUP estimates than in the positions to which it converged. Hence, it was not problems with the optimisation algorithm itself that caused the poor performance. Furthermore, it can be concluded that the initial guess is not the only problem causing poor results in calibrating Pass1.

GPS position

In the simulations it was shown that a uniform noise in the interval $[-2, 2]$ meters have a significant impact on the results. There are mainly three factors in the GPS that cause calibration error. Firstly, GPS equipment generally have errors in the size of meters, but since the boat mounted GPS is differential, as discussed in section 4.4, it is likely to have a lower error, potentially as low as 0.2 meters. Hence, it is probably not the intrinsic measurement error that is the major cause.

Secondly, it is not certain that the GPS equipment is located where the sound emitted from the boat is generated. For example, assume that the boat is seven meters long and that the engine, where most of the sound probably is generated, is located in the stern while the GPS is in the prow. This would introduce a bias of seven meters in the GPS measurements.

Finally, the hydrophones have a sampling rate of 30 kHz while the boat GPS have sampling rate of 1 Hz. In our model the boat is assumed to be still in between the GPS samles, hence most of the sound is allocated toward wrong positions. In the one second time window, the boat moves approximately 4.36 meters and this will impact both the sampled signal and the time delays for each hydrophone.

Recurrance of same τ in the plane

One possible source of error in the model is that, in each step of the optimisation algorithm the current position estimates only enters through the calculation of the time delays, τ_n, see equation (7.26). However, there could be several hydrophone positions in the plain that generate close to the same τ. This is due to the subtraction of the distance between the current source location and the reference point could scale different positions to almost the same time delays. This problem is likely to be more prominent if the initial guesses are far from the solution.

Reflections

There are also some less tangible uncertainties, such as reflections of the sound waves. When the sound waves are propagating they will be reflected on surrounding objects, in particular the ocean surface. This cause the sound waves to be reflected back toward the array and interfere with the incoming wave front. Depending on how strong the reflected signal is it could seriously impair the resolution of the beamformer. The same principle is problematic for rocks and other distortions of the ocean floor.

11.3 Response to problem formulation

In the problem formulation, see section 2.1, two main problems were defined. The first was concerned with whether the AELUP algorithm could be improved. The first part of this report concluded that instead of updating the AELUP estimates the results were maintained. However, this is more due to that these estimates were considered to be *good enough* by the FOI rather than *better* than the results produced by the AELUP-MM or the AELUP-CM algorithms. Hence, the final answer to the question is that the estimates probably can be improved, but that it is not necessary.

The second problem was if it was possible to develop an algorithm to calibrate the array based on the powerboat data. The results from Pass2 show that it is indeed possible. On the other hand Pass1 shows that the method does not appear robust enough to work for all arrays. Hence, it could be wise to research the method further before it is implemented on a wide scale in practice. The method does show great promise but the authors lack information about the trade-offs between for example high calibration accuracy and the cost of doing pinged experiments, and can therefore not give a recommendation whether to advance the project or not.

11.4 Suggestions for further research

In this thesis the main area of research have been to find a method for calibrating array positions based on a signal generated by a powerboat. The proposed method build around optimising over the output from a delay-and-sum beamformer. However, it would also be interesting to see what results can be generated by other beamforming methods. The difference compared to the delay-and-sum beamformer would be to choose the spatial filter in equation (7.13) differently. One example could be the Minimum Variance Distortionless Response (MVDR) Beamformer, see for example (Van Trees 2004, chapter 6).

A possible way forward, which theoretically would make the nested models gain in statistical efficiency would be to jointly estimate all nests rather than using the mean of the estimated results. However, due to that the energy varies greatly between design frequencies some type of SNR-weighting would be needed. The authors have made some attempts at this type of weighting but the results have always come

out worse compared to taking the mean value of the estimated positions. Despite this, it is believed that this is a possible area for improvement.

Another important area for future research would be to develop methods for estimation of the variance in the estimates. The variance of the current estimates is unknown, and adding to the problem is that the optimisation algorithms generally stopped prematurely. Therefore, more investigation into how and if the variance could be estimated would be highly relevant.

Furthermore, it would be interesting to see how robust the method is to different circumstances. Different circumstances could for example mean different sound speeds, different temperatures, more uncertainty in the GPS coordinates or different background noise. In practice, it is essential to develop a method that is robust to such changes as the Baltic Sea is not constant. A great combination would be to get estimates of the variance, as discussed in the previous paragraph, and try to combine this with more experiments to see if the findings hold under changing circumstances.

If implemented in practice, the idea would be to circle the array with the powerboat and then estimate the positions without ever using pings. Hence, results like the one for Pass1 could be grievous for the life long performance of the array. One interesting method, that does not require additional experiments, would be to first partition part of the powerboat data to use for validation. The validation would then work by taking the estimated hydrophone positions and try to estimate the direction of arrival for the incoming powerboat signal. If these DOA estimates were then compared to DOA estimates for the nominal positions it would be possible to determine if the calibration was successful.

Bibliography

Chen, Jin et al. (2013). "Offshore towed hydrophone linear array: principle, application, and data acquisition results". In: *EURASIP Journal on Wireless Communications and Networking* 2013.1, p. 35. ISSN: 1687-1499. DOI: 10.1186/1687-1499-2013-35.

Rabinovich, Victor and Nikolai Alexandrov (2012). *Antenna arrays and automotive applications*. Springer Science & Business Media.

Stoica, Petre and Randolph L Moses (2005). *Spectral analysis of signals*. Vol. 452. Pearson Prentice Hall Upper Saddle River, NJ.

Van Trees, H.L. (2004). *Detection, Estimation, and Modulation Theory, Optimum Array Processing*. Wiley. ISBN: 9780471463832.

Liu, W. and S. Weiss (2010). *Wideband beamforming: concepts and techniques*. Wiley.

Christensen, JJ and J Hald (2004). "Technical review beamforming". In: *Bruel&Kjear, Danmark*, pp. 3–12.